DESIGN OF HIGH FORCE DENSITY FISHBONE-SHAPED ELECTROSTATIC ACTUATOR USING FINITE ELEMENT

MEGAT MUHAMMAD IKHSAN BIN MEGAT HASNAN

(KGA120043)

DISSERTATION SUBMITTED IN FULLFILLMENT OF THE REQUIREMENTS FOR THE DEGREE OF MASTER OF ENGINEERING SCIENCE

FACULTY OF ENGINEERING
UNIVERSITY OF MALAYA
KUALA LUMPUR

2014

University of Malaya

ORIGINAL LITERARY WORK DECLARATION

Name of Candidate: **MEGAT MUHAMMAD IKHSAN BIN MEGAT HASNAN**

Registration/Matric No: **KGA120043**

Name of Degree: **Master of Engineering Science**

Title of Dissertation ("this Work"):

Design and Finite Element Analysis of High Force Density Fishbone-shaped Electrostatic Actuator

Field of Study: **Electrical Engineering**

I do solemnly and sincerely declare that:

(1) I am the sole author/writer of this Work;
(2) This Work is original;
(3) Any use of any work in which copyright exists was done by way of fair dealing and for permitted purposes and any excerpt or extract from, or reference to or reproduction of any copyright work has been disclosed expressly and sufficiently and the title of the Work and its authorship have been acknowledged in this Work;
(4) I do not have any actual knowledge nor do I ought reasonably to know that the making of this work constitutes an infringement of any copyright work;
(5) I hereby assign all and every rights in the copyright to this Work to the University of Malaya ("UM"), who henceforth shall be owner of the copyright in this Work and that any reproduction or use in any form or by any means whatsoever is prohibited without the written consent of UM having been first had and obtained;
(6) I am fully aware that if in the course of making this Work I have infringed any copyright whether intentionally or otherwise, I may be subject to legal action or any other action as may be determined by UM.

Candidate's Signature **Date:**

Subscribed and solemnly declared before,

Witness's Signature **Date:**

Name:

Designation:

ABSTRACT

This study presents the design and evaluation of high force density fishbone shaped electrostatic comb drive actuator. The fishbone shaped comb drive actuator has structure similar to fishbone, which is intended to increase the capacitance of the electrodes, and hence increase the electrostatic actuation force. Two-dimensional finite element analysis was used to simulate the motion of the fishbone shaped electrostatic comb drive actuator, and compared against the performance of a straight sided electrostatic comb drive actuator. The performances of both designs are compared by evaluating the displacement and electrostatic force for both systems. For both cases, the active area and the minimum gap distance between the two electrodes were kept constant. Performance comparison of the fishbone shaped electrostatic comb driver and straight finger electrostatic comb driver are demonstrated with an active area of 800x300 μm^2, which contained 16 fingers of fishbone shaped actuators and 40 fingers of straight sided actuators, respectively. Through the modeling and simulation, improvement of drive force of the fishbone shaped electrostatic comb driver is approximately 485% compared to the straight comb finger of conventional electrostatic comb driver. These results indicate that the fishbone actuator design provides good potential for applications as high force density electrostatic micro actuator in MEMS systems. The fishbone shaped comb driver introduced in this work shows a characteristic stepped force profile versus finger engagement compared to the conventional straight sided comb driver. However, a cogging effect was demonstrated, due to the negative force components of the fishbone shaped comb driver. So, a finger shifting method in comb arrays was introduced to mitigate the negative force profile, in order to ensure more linear electrostatic force profile.

ABSTRAK

Kajian ini membentangkan reka bentuk dan kajian tentang elektrostatik aktuator yang berbentuk tulang ikan dengan daya berketumpatan tinggi. Elektrostatik aktuator tersebut mempunyai struktur berbentuk seperti tulang ikan yang mana bertujuan meningkatkan kapasiti bagi elektrod dan kemudian meningkatkan daya elektrostatik yang dihasilkan aktuator. Analisa elemen terhingga dua dimensi digunakan untuk simulasi pergerakan bagi elektrostatik aktuator berbentuk tulang ikan kemudian dibandingkan dengan prestasi elektrostatik berbentuk lurus di sisi. Prestasi untuk kedua-dua reka bentuk dibandingkan dengan kajian terhadap perubahan sesaran dan daya elektrostatik untuk kedua-dua sistem. Untuk kedua-dua kes, kawasan aktif dan ruang jarak minimum bagi dua elektrod dipastikan mempunyai jarak yang sama. Perbandingan prestasi untuk elektrostatik aktuator berbentuk tulang ikan dan elektrostatik aktuator berbentuk lurus di demonstrasi dengan kawasn aktif 800 x 300 μm^2, yang mana mempunyai 16 set aktuator berbentuk tulang ikan dan 40 set aktuator berbentuk lurus di tepi. Melalui proses pembentukan dan simulasi, kemajuan untuk daya gerak yang terhasil bagi aktuator berbentuk tulang ikan ialah 485% berbanding aktuator berbentuk lurus. Keputusan ini menunjukkan yang reka bentuk aktuator yang berbentuk tulang ikan mempunyai potensi yang bagus dalam aplikasi mikroaktuator yang memerlukan daya elektrostatik yang berketumpatan tinggi dalam sistem "MEMS". Elektrostatik aktuator berbentuk tulang ikan yang diperkenalkan dalam kajian ini menunjukkan profil daya bertingkat melawan perubahan sesaran berbanding aktuator konventional yang lurus di sisi. Kesan "cogging" telah didemontrasi disebabkan komponen daya negatif yang dihasilkan aktuator berbentuk tulang ikan. Method peralihan dalam barisan set aktuator diperkenalkan untuk mengurangkan kesan profil daya negatif untuk memastikan profil daya elektrostatik yang lebih lurus.

ACKNOWLEDGEMENT

All praise is to be Almighty Allah S.W.T, The merciful and Beneficent for the strength, patience and perseverance which blessings throughout the entire time until completion of this dissertation. Peace be upon our prophet Muhammad S.A.W, who has preached light to mankind.

My sincere gratitude goes to my supervisor Dr Suhana Mohd Said for support, guidance and encouragement throughout my Master's program. Special thanks to my co-supervisor Dr Faizul Mohd Sabri from Department of Mechanical Engineering University Of Malaya for granting me the opportunity to gain invaluable experienced with new field as guidance in designing and sharing knowledge. We acknowledge this research is supported under Fundamental Research Grant Scheme (FRGS):FP021/2012A, HIR-MOHE research grants UM.C/HIR/MOHE/ENG/29, RP104D-13AET research grants University of Malaya.

I am also indebted to my parents; Mr Megat Hasnan bin Megat Din and Mrs Norehan binti Alang Abdul Shukor for tolerance, understanding, moral support and grateful sacrifice. Special thanks to Nurhidayati Binti Ahmad Syufai for ideas, support and understanding until the end of this study.

Thanks to the members of the Solid State Nanodevices laboratory and NanoMicro Engineering laboratory of the Faculty of Engineering, University of Malaya for their suggestions and valuable discussions during the course of this work.

I am also grateful to all unnamed people, who have directly or indirectly helped me in completing my research. Their contribution is highly appreciated.

The kindness and corporation from all would always be remembered. May Almighty Allah bless us with His mercy.

TABLE OF CONTENTS

LIST OF FIGURES

LIST OF TABLES

LIST OF SYMBOLS AND ABBREVIATIONS

Nomenclature	Description
$\mathbf{E}$	Electrostatic field intensity
$\mathbf{V_0}$	Actuation potential bias
$\boldsymbol{\varepsilon_0}$	Constant permittivity of free space
$\boldsymbol{c}$	Capacitance
$\mathbf{F}_{\boldsymbol{ez}}$	Electrostatic force
$\mathbf{W}_{\boldsymbol{e}}$	Electrostatic energy
$\boldsymbol{n}$	Number of comb fingers
$\boldsymbol{g}$	Gap between fixed and moving electrode
$\boldsymbol{K}$	Spring constant
$\boldsymbol{x}$	Cartesian axis in the X-axis
$\boldsymbol{y}$	Cartesian axis in the Y-axis
$\boldsymbol{z}$	Cartesian axis in the Z-axis
$\boldsymbol{W}$	Width
$\boldsymbol{R}$	Constant separations between arrays of small protruding fingers connected within the electrode
$\mathbf{\theta}^{\circ}$	Angle relative to the position of the electrode
$\boldsymbol{F_s(n)}$	Finger shifting value
$\boldsymbol{l}$	Length
a, b, c* and *d	Parameters of fish bone shape design
$\boldsymbol{E}$	Young's Modulus
$\mathbf{T}$	Thickness

LIST OF APPENDIX

CHAPTER 1

INTRODUCTION

1.1 Background

Actuators are used to convert non-mechanical input energy into mechanical output energy. Actuators can be used in different scales, ranging from macroscopic actuation through electromagnetic motors, hydraulics and pneumatics, to microscopic actuation where the actuators are of the order of microns for MEMS applications. In MEMS applications, actuators are used to achieve positioning (Sun, Nelson, Potasek & Enikov, 2002), such as positioning a cantilever tip to perform as micro grippers to move miniature objects (Kim, Pisano, Muller & Lim, 1992), or to access a specific data point in data storage systems such as in the "Millipede project" (Eleftheriou et al., 2003). The main parameters that need to be considered for micro actuator performance include displacement, response time, load capacity, actuation force, resolution, degrees of freedom and size (Ahmed & Moussa, 2003; Chiou, Kuo, Lin, Chang & Huo, 2008; Engelen, Lantz, Rothuizen, Abelmann & Elwenspoek, 2009; Chow & Lai, 2009).

The most common actuators are piezoelectric actuators, electromagnetic actuators, electrostatic actuators, thermal actuators, and electrochemical actuators, each with their respective advantages and drawbacks (Hu, Hu, Wei & Xie, 2010; Krishnan & Saggere, 2012; Wang ,Yang & Yan, 2012; Bell , Fleck & Spearing, 2005; Olfatnia, Sood, Gorman & Awtar, 2013). For example, electromagnetic actuators possess a high efficiency in converting electrical energy into mechanical work, but are bulky and require a high operating voltage (Lantz, Rothuizen, Drechsler, Haberle & Despont, 2007). On the other hand, piezoelectric actuators provide a high actuation force and speed, but have low intrinsic displacement (Conway & Kim, 2004; Sabri, Ono and Esashi, 2009). Electrostatic

actuators have some favorable performance characteristics, such as a large displacement, as demonstrated by (Grade, Jerman & Ken, 2003; Liu & Kenny, 2001). However, a main drawback of the electrostatic micro actuator is large active area, as a typical electrostatic actuator configuration comprises of a large array of interdigitated electrodes which occupy a large surface area.

The most common comb drive actuator design consists of straight sided comb fingers where one half of the comb electrode is static whilst the other half is movable and hence provides the actuator motional force (Tang, Lim & Howe, 1992; Tang, Nguyen & Howe, 1989). The magnitude of the force is dependent upon the applied voltage as well as the geometry of the finger (Jaecklin, Linder, De Rooij & Moret, 1992; Tang, Nguyen, Judy & Howe, 1990). Several previous researchers have investigated variations in the comb shape design (Ye, Mukherjee & MacDonald, 1998; Jensen, Mutlu, Miller, Kurabayashi & Allen, 2003). (Rosa, Dimitrijev & Harrison, 1998) have investigated variations in the design of high force actuators through the use of angled comb fingers. (Ye, Mukherjee & MacDonald, 1998; Jensen, Mutlu, Miller, Kurabayashi & Allen, 2003) reported designs with linear, quadratic and cubic force-engagement behavior. (Jensen, Mutlu, Miller, Kurabayashi & Allen, 2003) had developed and validated a simple analytical model based on the rate of change of capacitance with respect to the finger engagement for several comb shapes, including a saw-tooth design. One of the applications for electrostatic actuator is the micro-gripper or microtweezer as proposed by (Kim, Pisano, Muller & Lim, 1992). In this study, design and optimization of a fishbone shaped actuator presented. The fishbone design has been shown to have high force density potential for micro tweezers, the stepped lateral force in the translational direction is optimized to ensure high force density and smooth translational motion.

Therefore, this study proposes a design which aims to achieve a high displacement, and high force density electrostatic comb drive actuator, which is not limited by the issues stated above. This proposed design is fundamentally a branched actuator resembling a fishbone, where a 'backbone' has smaller fingers protruding out of it. This design is intended to replace the straight-sided comb actuator conventionally used. Introduction of the branched 'fishbone' structure increases the cross-sectional area of the electrodes, and correspondingly, the capacity of the structure. Given that the electrostatic force is the gradient of the electrostatic energy, and in turn, the electrostatic energy is proportional to the capacity under constant voltage conditions, the electrostatic force is inferred to increase with a corresponding increase in capacity. In this paper, the fish-bone shape of electrostatic comb drive is proposed to replace the conventional comb driver for high force density performance, through the increase in the cross-sectional area due to the fishbone structure. This study will first explain the fundamental design of the fishbone actuator, followed by the performance analysis of this design compared to the straight sided actuator.

1.2 Research Objectives

There are three main objectives of this research.

1. To validate the simulation results of conventional actuator with available literature.
2. To design and simulate fish bone shaped electrostatic actuator.
3. To characterize the performance of fishbone shaped electrostatic actuator.
4. To optimize the force density performance of fish bone shaped electrostatic actuator.

1.3 Layout of Dissertation

Chapter 1 explains a brief background of the research, the research objectives as well as layout of thesis is presented in this chapter

Chapter 2 reviewed the state of art in this area of studies. A large number of recently published journal articles have been critically reviewed. In this chapter some relevant information are presented related to basic principle and operation of the conventional electrostatic comb driver actuator. The design of existing actuator and the technology behind that are covered and discussed.

Chapter 3 explains the method of analysis used to simulate the fish bone shaped design using COMSOL Multiphysics simulation tools. All the simulation and optimization process and steps are explained in detail in this chapter. The detail about fish bone shaped comb drive actuator design, parameters and concept also explained in Chapter 3. In this chapter, the problem may be faced by the design is also mentioned and the solution to overcome it is proposed.

The data, results and discussion from investigation of fish bone shaped comb drive actuator are compiled and documented in Chapter 4.

Chapter 5 consists of concluding remarks from the analysis performed based on the objectives of the thesis. The best parameters for the fish bone shaped comb driver actuator design are concluded based on the optimization result and analysis.

CHAPTER 2

LITERATURE REVIEW

2.1 Actuator

Actuators are systems that convert energy to motion. In micro electromechanical system (MEMS) applications, actuators are used for micro positioning, micro gripper, and resonator. Examples of actuator are electrostatic actuators, electromagnetic actuators, thermal actuators and electrochemical actuators (Bell, Lu, Fleck, & Spearing, 2005).

2.2 Basic Static Capacitor

A capacitor is made of two conductive solid elements (the electrodes) separated by a dielectric non-conductive environment such as gas, solid, liquid. If a voltage is applied between the conductive parts, an electric field will be created across the dielectric material. Electrical charges will agglomerate on the conductive parts, corresponding to an equilibrium made with the electric field (Brown & Hemingway, 1995).

The capacity is the ability to store a quantity of electrical charges, depending on the voltage difference between the electrodes forming the capacitance. As shown in Figure 2.1, once the charges reach the equilibrium point, the capacity is loaded. Hence, if the voltage supply has been cut off, and the capacitance is in an open circuit, it maintains the voltage difference between the electrodes, and if the branch is in a closed circuit position, it will give back its electrical charges, generating current, until it is completely unloaded as shown in Figure 2.1. Loading and unloading imply electrical charges displacement and consequently electrical current.

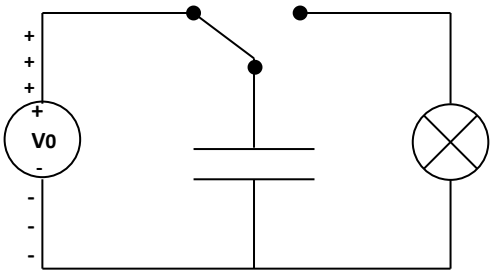

(a)

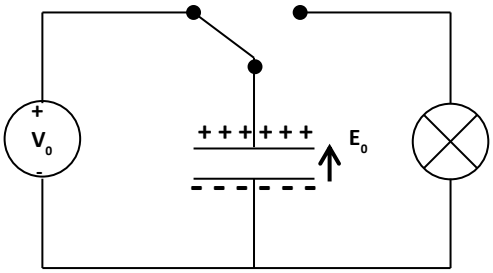

(b)

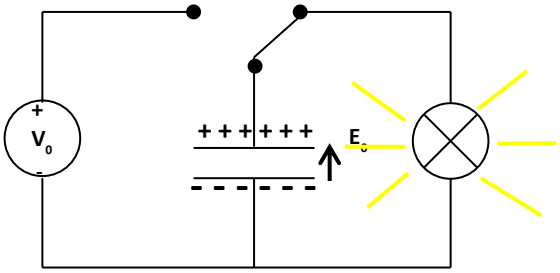

(c)

Figure 2.1: Capacitor charge loading and unloading (a) electrical charges, (b) capacity loading, and (c) capacitor complete unloaded

The parallel plate capacitor geometry consider two rectangular plates parallel to the plane defined by the (X,Y) axes, of size L by W, separated by a thickness d along z axis, of air having an electrical permittivity of ε_0. To simplify notations, the term area, A=LW denote the surface of the plates.

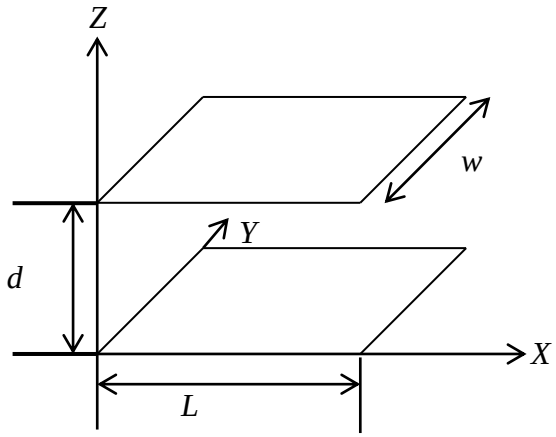

Figure 2.2: Two rectangular plates forming a capacitor

Consider that two plates are perfectly conductive.

$$E_z = E_z(z)\, u_z \qquad \text{(Equation 1)}$$

Capacitive calculation involves a relation between the voltage across the electrode and the electrical charges on the plates. For both elements, the electric field is used to get the values (Lagouge, 2009).

2.2.1 Relationship between electric field and voltage

According to the electric field definition for E:

$$E = -\nabla V \qquad \text{(Equation 2)}$$

However air does not contain electrical charges, so using Maxwell-Gauss equation $\nabla . E$:

$$\nabla . E = \rho \varepsilon_0 = 0 \qquad \text{(Equation 3)}$$

So that E is a constant vector $E_0 u_z$. This implies for the electrical potential the following solution:

$$V_0(z) = -E_0 . d + V(0) \qquad \text{(Equation 4)}$$

Considering that the bottom plate is at a potential V = 0,

$$\Delta V = -E_0 . d \qquad \text{(Equation 5)}$$

2.2.2 Relationship between electrical field and charges

The charges were accumulating on the conductive plates. Using Maxwell-Gauss equation, inside the box,

$$\nabla . E = \rho \varepsilon_0 \qquad \text{(Equation 6)}$$

Finally, C is:

$$C = \varepsilon_0 A d \qquad \text{(Equation 7)}$$

Where C is the capacity for parallel plates

2.3 Electrostatic Force

An electrical charge creates an electric field around it. Conversely, an electric field exerts a force to charged particle. The main problem of electrostatic effect is the electrostatic force is inversely proportional to the square of the distance between the two charged bodies.

The electrostatics force is the most widely used force in the design of MEMS device. In industry, it is used in applications such as micro resonators, switches, micro mirrors, and accelerometers.

The electrostatic force depends largely on the size of the structures and the distance between electrodes. So, for large electrode surfaces compared to distance to travel, electrostatic actuation has a large advantage. However, given that the electrostatic force is depend to the square of the distance. Therefore, a large actuation distance will require a large actuation voltage to exert the driving force on the actuator. This is one of the main problems with this electrostatic force principle where the actuation voltage is usually high, in scales tens, and even hundreds of volts. High voltages may be easily large integrated in a system, but not on a very compact integrated system (Rivlin & Elata, 2012).

An interesting point is the fact that the electric circuit is capacitive. Given the typically low capacitance rating that the power consumption is relatively low. The nature of the material between electrodes (water for example) is conductive at low frequencies, so electrostatic actuation cannot be used in these conditions. Void and neutral gases are the best environments for the electrostatic actuator system (Lagouge, 2009)

2.4 Electrostatic Microactuator

Most micro electromechanical systems (MEMS) use electrostatic actuator as actuation method because of the simple principle and ease of fabrication methods. Electrostatic actuator is a system that changes electrostatic energy to motion.

2.4.1 Parallel plate electrostatic actuator

The operation of a comb drive actuator is first compared with the operation of a parallel electrostatic actuator. In the parallel electrostatic actuator as shown in Figure 2.3, two electrodes possess two parallel surfaces facing each other. At least one of the two electrodes moves along the direction of the applied electrical field. In this case, the capacitance *C* is inversely proportional to the gap between the electrodes where capacitance is

$$C = \frac{\varepsilon A}{g} \qquad \text{(Equation 8)}$$

and the resultant electrostatic energy $\mathbf{W}_e$ is directly proportional to the capacitance under constant voltage conditions (Abarca et al., 2015).

$$\mathbf{W}_e = \frac{1}{2} C \mathbf{V^2} \qquad \text{(Equation 9)}$$

In turn, the relationship of the electrostatic force $\mathbf{F}_{ez}$ and the electrostatic energy is given by

$$\mathbf{F}_{ez} = -\frac{\partial \mathbf{W}_e}{\partial z} \qquad \text{(Equation 10)}$$

However, parallel actuators normally have very limited displacement range. The direction of the displacement along the direction is limited by the electrode gap (*g*), which is defined

as the shortest distance between two electrodes. The electrostatic force (**F**) generated in a unit area is (Liu & Kenny, 2001).

$$\mathbf{F} = \frac{\varepsilon \mathbf{V}^2}{2g^2} \qquad \text{(Equation 11)}$$

Where $\boldsymbol{\varepsilon}$ is the dielectric constant, **V** is voltage, g is minimum distance between fixed and moving electrode. The electrostatic force generated by a parallel electrostatic actuator is therefore highly nonlinear as it is a function of the electrode gap (g). Moreover, a parallel plate actuator usually has a collapse voltage, beyond which the electrodes will collide into each other. The positive feedback when the actuator deflects cause instability in the parallel plate actuator where the electrode gap is 1/3 of the initial gap (Harouche & Shafai, 2005)

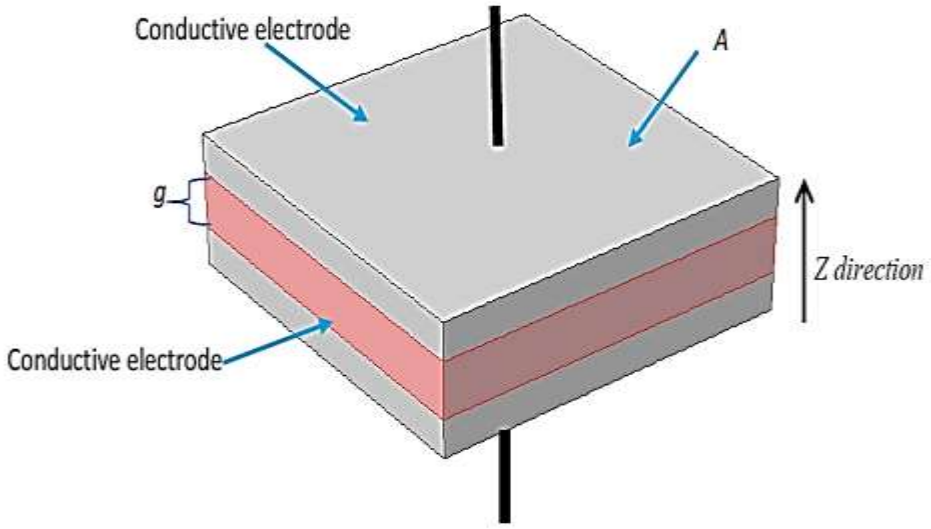

Figure 2.3: Example of parallel plate capacitor

The occurrences of different charges result from different electric potential on both side of the capacitor plate caused the attractive force between the plates.

2.4.2 Conventional comb drive actuator

Electrostatic comb drivers were designed in order to overcome the nonlinear voltage-displacement characteristics of the parallel electrostatic actuator (Osonwanne & Clark, 2010). A comb electrostatic actuator as shown in Figure 2.4 generates an electrostatic force to drive a movable member of the comb driver. However the existing electrostatic comb drivers have their own challenges. For example, a comb driver usually occupies more space than that of a parallel plate actuator and has a smaller electrostatic force density due to the large active area occupied by the comb structure. The width of comb fingers should be as small as possible to enhance the force density of the comb driver (Bronson, 2007). Comb drive actuators are used to produce large displacement at low driving voltages.

The mechanism of operation for electrostatic actuators can be described as follows:
A set of interdigitated electrodes (or combs) of opposite polarities are arranged as shown in Figure 2.4 in order to set up an electric field. One set of the combs is fixed, whilst the other set is allowed to move. The resulting electrostatic field produces an electrostatic force to drive the motion of the moveable set of combs. This electrostatic force has components in the x-y plane (in-plane motion) and the z-plane (out-of plane motion). Typically, the "useful" force is the component along the longitudinal axis of the electrostatic combs, whilst the components of force in the other directions are considered undesirable and lead to side snap-in (collision between fixed and moving electrodes). However, there have also been novel designs where this "side snap-in" can be utilized for a higher degree of freedom of motion.

The electrostatic actuators are useful for producing a large displacement at low driving voltage (Bell , Lu , Fleck & Spearing, 2005). However, its force density only ranges from low to moderate, owing to its large surface area. Strategies to increase the force density include increasing the number of comb fingers, increasing the electrical potential, and reducing the gap between the fixed and moving electrodes. However, each of these strategies have their own drawbacks: increasing the number of comb fingers result in an increase in active area, increasing the potential corresponds to an increase in driving voltage, and reducing the gap width has a limitation in terms of fabrication capability (Harouche & Shafai, 2005)(Osonwanne & Clark, 2010). Therefore, it is difficult to fabricate electrodes beyond a minimum size, and correspondingly, small gap (2-3 μm). In addition, a small gap also result in a higher possibility of lateral instabilities, where translational motion intended to be in say, the x-direction also results in significant deflection in the y-directions and z-directions, hence causing the two sets of combs to collide (Bronson, 2007).

The equation governing the drive force **F** generated by an electrostatic comb drive is given below (Legtenberg , Groeneveld & Elwenspoek, 1996):

$$\mathbf{F} = \frac{n\varepsilon t}{g}\mathbf{V}^2 \qquad \text{(Equation 12)}$$

Where n is number of fingers, ε is electrical permittivity, t is finger thickness, g is gap between fingers, and **V** is voltage applied. Note that n, t, and g are the parameters related to the physical dimension of the comb actuator. The force generated by the standard comb drive actuator, remains constant even though the engagement distance changes O_L with a uniform gap g between the fixed and moving electrodes (Jaecklin, Linder, De Rooij & Moret, 1992)

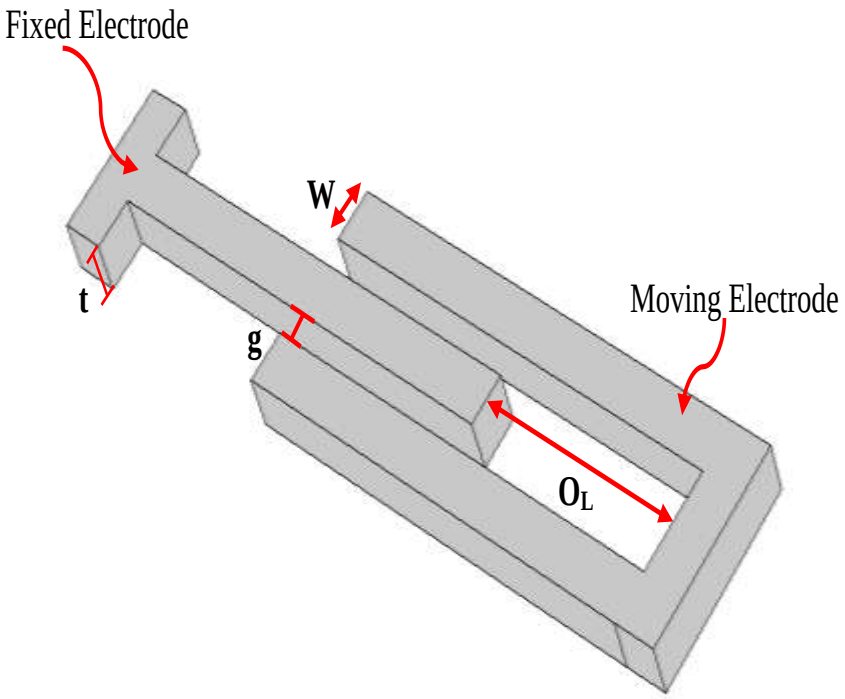

Figure 2.4: Example of conventional straight sided comb driver

2.5 Improvement of Force Density

Theoretically, from the governing equations the improvement of the drive force can be done by several ways. First, by increasing the number of comb fingers **n** which also consume more space. Second, by increasing the voltage potential **V** which will require more power used and at certain level it will generate heat loss. Minimum distance between the moving and fixed electrode **g** also can be decreased to increase drive force but the disadvantages is the minimum distance cannot be reduced too small because of the fabrication limitation and lateral instability of the actuator which require more flexible spring design to support the moving electrode and avoid short circuit (Hu et al., 2010).

2.5.1 Stepped and tapered Design

From (Engelen, Lantz, Rothuizen, Abelmann & Elwenspoek, 2009) two comb finger shapes are investigated; a tapered shaped and stepped shape, both shown in Figure 2.5

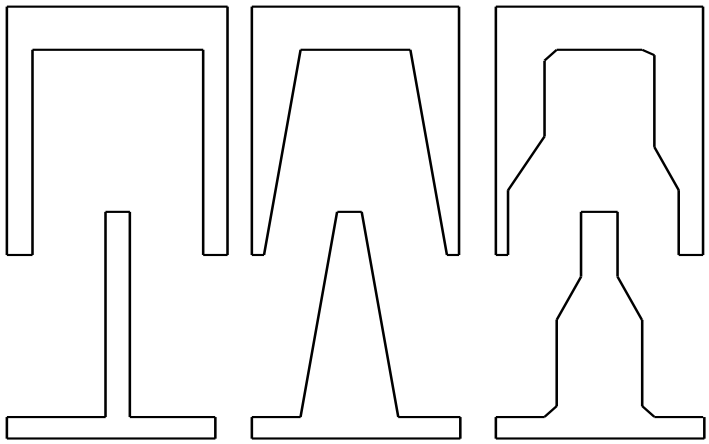

Figure 2.5: The three investigated finger shapes (a) conventional, (b) stepped, and (c) tappered (Engelen et al., 2009)

For straight fingers, the necessary change in capacitance $\frac{\partial C}{\partial x}$ is caused by increasing of finger overlap; for gap narrowing finger shape, and extra term to decreasing gap distance between fingers adds to the capacitance change which result increasing drive force.

$$F = \frac{1}{2} N \frac{\partial C}{\partial x} V^2 \qquad \text{(Equation 13)}$$

From the study, the device using stepped fingers reaches a 25% larger displacement than the device using tapered fingers.

2.5.2 Jagged edge shaped comb driver design

From (Harouche & Shafai, 2005), the jagged edge shape comb driver in Figure 2.6 were introduced to achieve more linear force-engagement profile .The present work discusses move-and-lock mechanism based on jagged edge shape comb drive design .The main use of the design is for micro tweezers actuator for application in area such as biological sample handling, MEMS assembly processes and other activities where precision micromanipulation and force-controlled interaction are required (Wierzbicki et al., 2006).

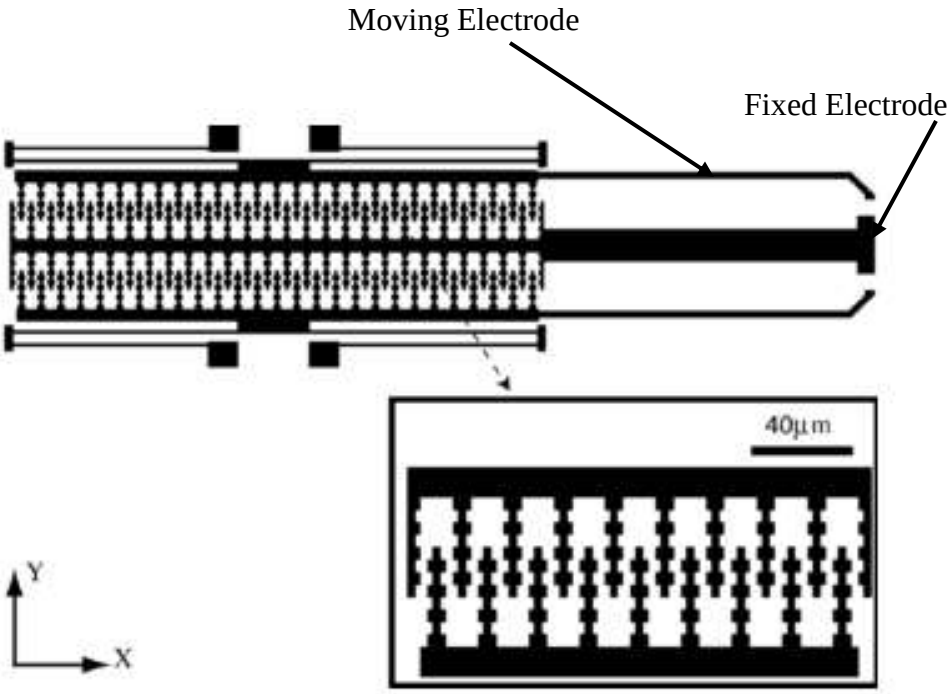

Figure 2.6: Illustration of the design for the shaped comb drive as a micro tweezers actuator. The blow-up image shows a representation of a jagged-edge comb drive (Harouche & Shafai, 2005)

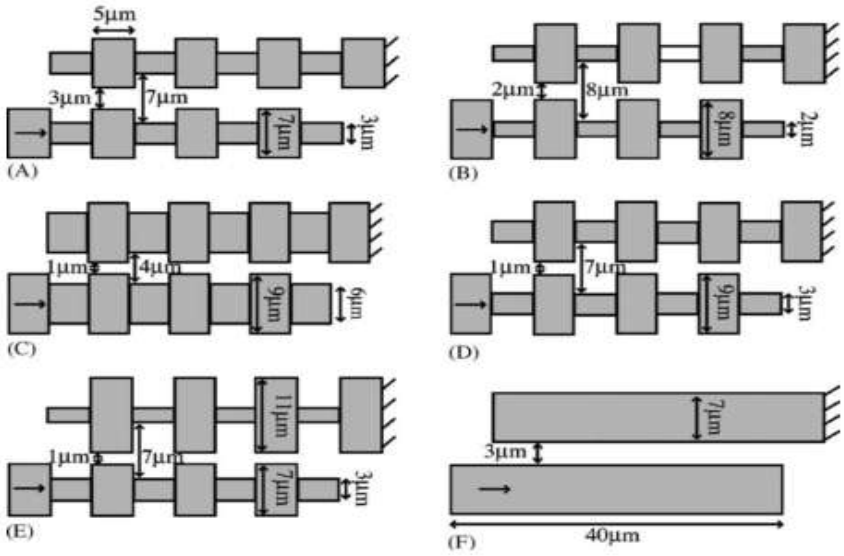

Figure 2.7: The five jagged-edge comb designs analyzed (Harouche & Shafai, 2005)

Results for the last analysis are shown in the context of all simulations. Figure 2.8 shows combined plots of displacement gradient with respect to actuation voltage. Note that the asymmetric 7:1 design shows two clear points of inflection. The first step in displacement occurs at about 40V. By observing the slope of the curve, it is possible to infer an increase in velocity, which implies that the movable comb finger accelerates. It then decelerates to a constant, stable and small displacement. Ideally, the structure should almost lock in place preventing any Y-direction movement. When the input potential reaches 150V another surge in acceleration happens. At this point, the total amount of displacement is larger than in the previous engagement. The general behavior of the 7:1 symmetric design was similar, but the points of inflection are not as accentuated and the trough not as low, implying more slippage. The optimizations of the design are done based on the maximum to minimum gap relationship. Based on the investigations the optimizations resulted from asymmetric 7:1 gap ratio for a device with 2µm thick structural. Figure 2.9 illustrates the 7:1 designs in detail (Harouche & Shafai, 2005).

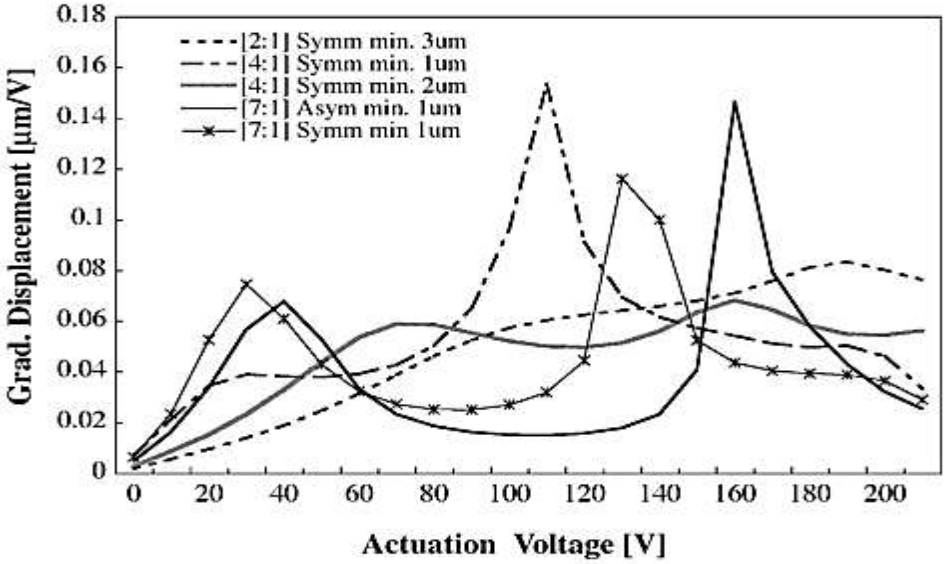

Figure 2.8: Comparison of differential displacements of all geometries investigated

(Harouche & Shafai, 2005)

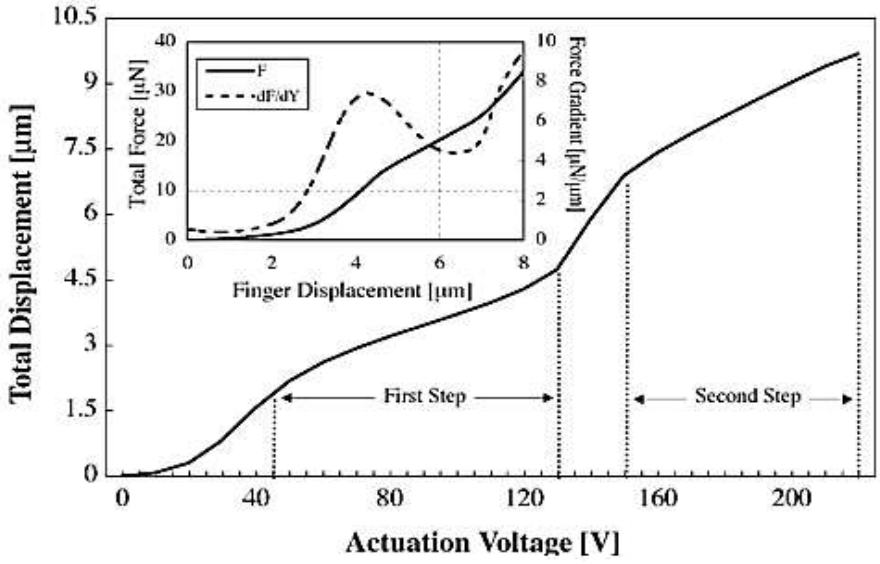

Figure 2.9: Analysis of the 7:1 symmetric design shape "D" (Harouche & Shafai, 2005).

2.5.3 Shaped comb fingers

From (Jensen et al., 2003), shaped comb fingers in Figure 2.10 represent a way to vary the gap between fingers because for the rectangular conventional comb finger, the geometry only results in a constant gap between fixed and moving fingers as they engage.

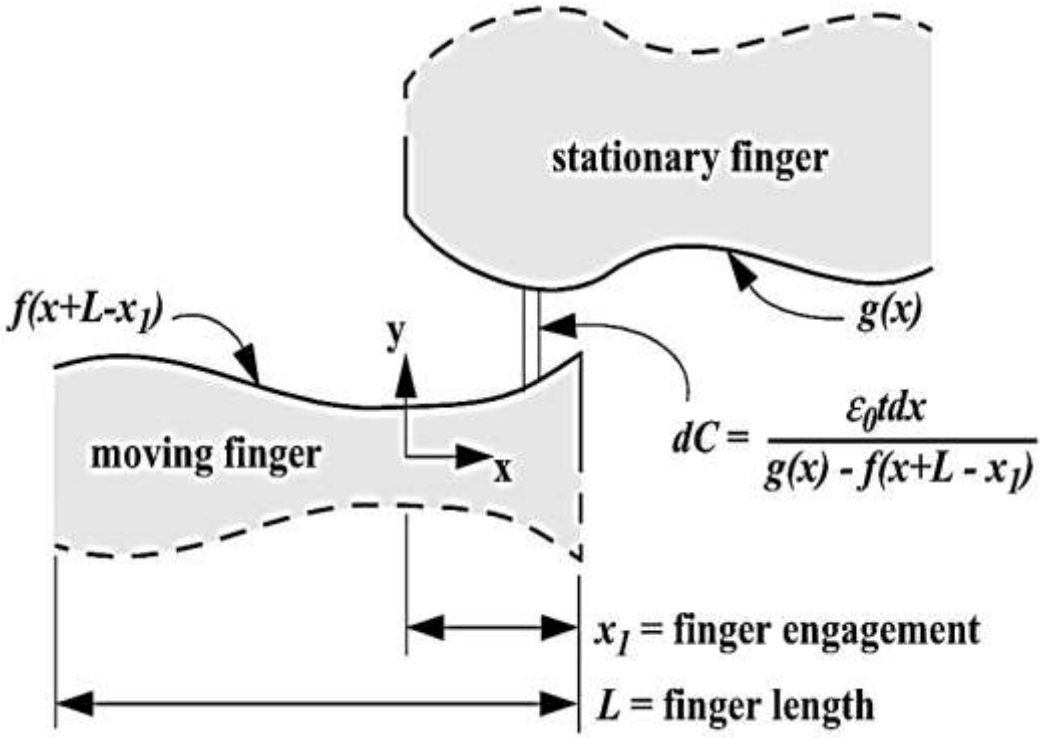

Figure 2.10: Illustration of engagement of arbitrarily-shaped fingers (Jensen et al., 2003)

The first comb finger design is the simple rectangular comb finger with a constant gap of 1 µm. This design was chosen to verify that a constant force relationship resulted. The next four finger designs, cases 2,3,4, and 5 shown in Figure 2.11 were derived from the earlier work by (Ye, Mukherjee, & MacDonald, 1998). As shown in Figure 2.12 they reported that designs 2 and 4 showed linear force engagement behavior ,while design 3,5 and 6 were cubic profile which result larger forces than linear force profile.

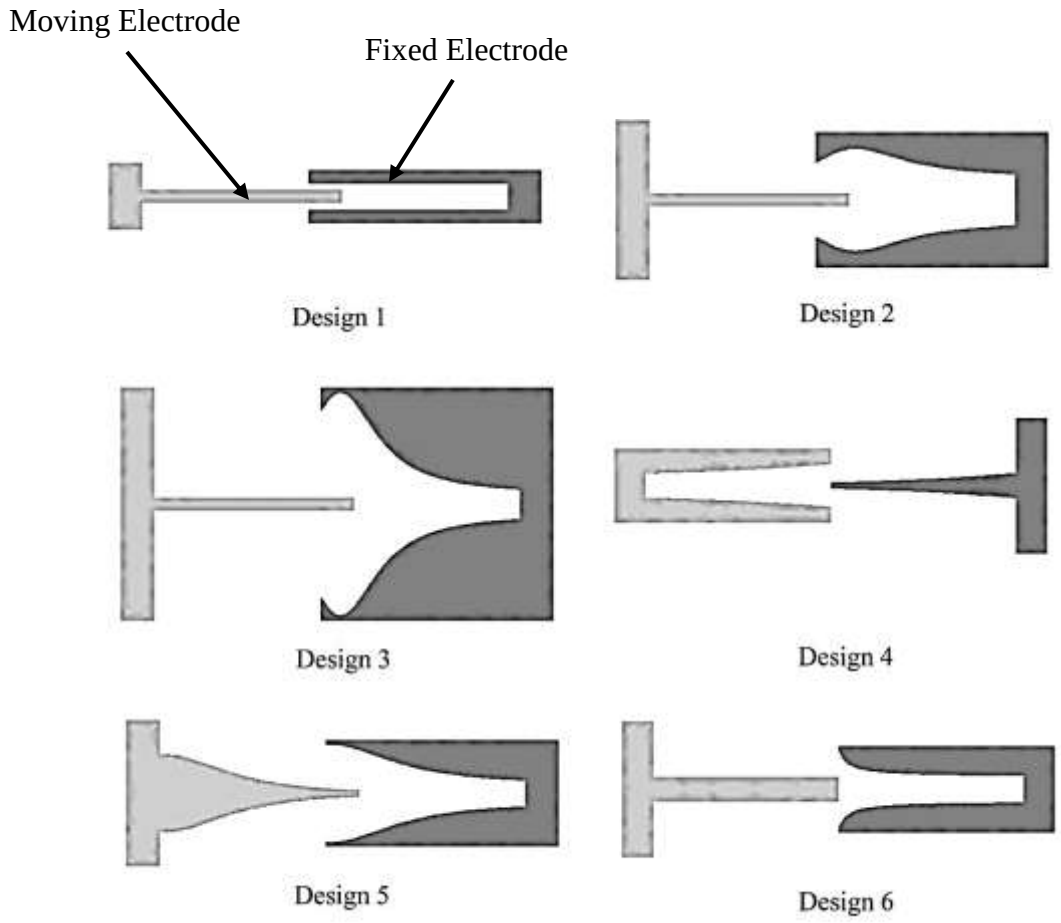

Figure 2.11: The six comb finger designs studied (Jensen et al., 2003)

The first comb finger design is the simple rectangular comb finger with a constant gap of 1 µm. This design was chosen to verify that a constant force relationship resulted. For the next four finger designs, cases 2,3,4 and 5,were derived from the earlier work by (Ye, Mukherjee & MacDonald, 1998). They reported that designs 2 and 4 showed linear force engagement behavior, while design 3 and 5 were cubic profile.

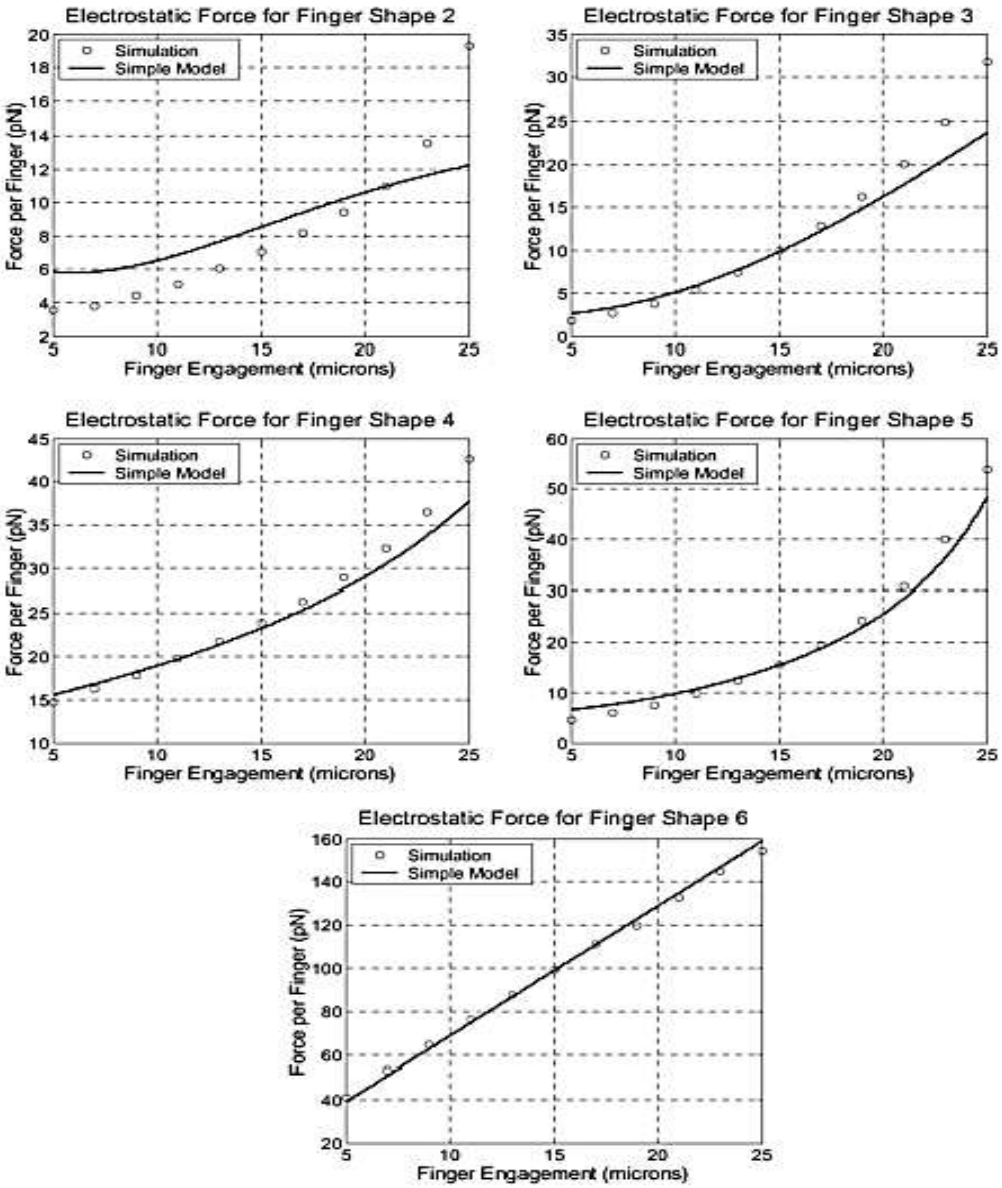

Figure 2.12: Graphs showing force acting on a single finger for each of the shaped fingers (Jensen et al., 2003)

2.5.4 Saw tooth comb driver

From the patent by (Huang, 2007), the author introduce a novel arrangement of interdigitated electrode saw tooth shaped comb as an electrostatic comb drivers. From (Rosa, Dimitrijev, & Harrison, 1998), the authors showed the performance of using angled comb drive, which possess a saw tooth like as shown in Figure 2.13 The performance of this angled comb driver showed higher performance than a straight conventional comb driver as shown in Figure 2.14 .The actuating force generated via an angled comb finger design can exceed that of a device using a rectangular design, since its output force increases parabolic with a diminishing comb finger gap. Despite a parabolic increase in actuating force, collision between opposing comb fingers is avoided due to the larger opposing force imposed by the support beam's spring constant, limiting the maximum achievable displacement.

Equation 14 illustrates a relationship between comb finger angle θ, allowable clearance (maximum displacement) and comb finger gap width, such that a compromise based on these parameters and the intended application need to be made before device design can take place.

$$\sin\theta = \frac{gap\ width(g)}{clearence(d)} \qquad \text{(Equation 14)}$$

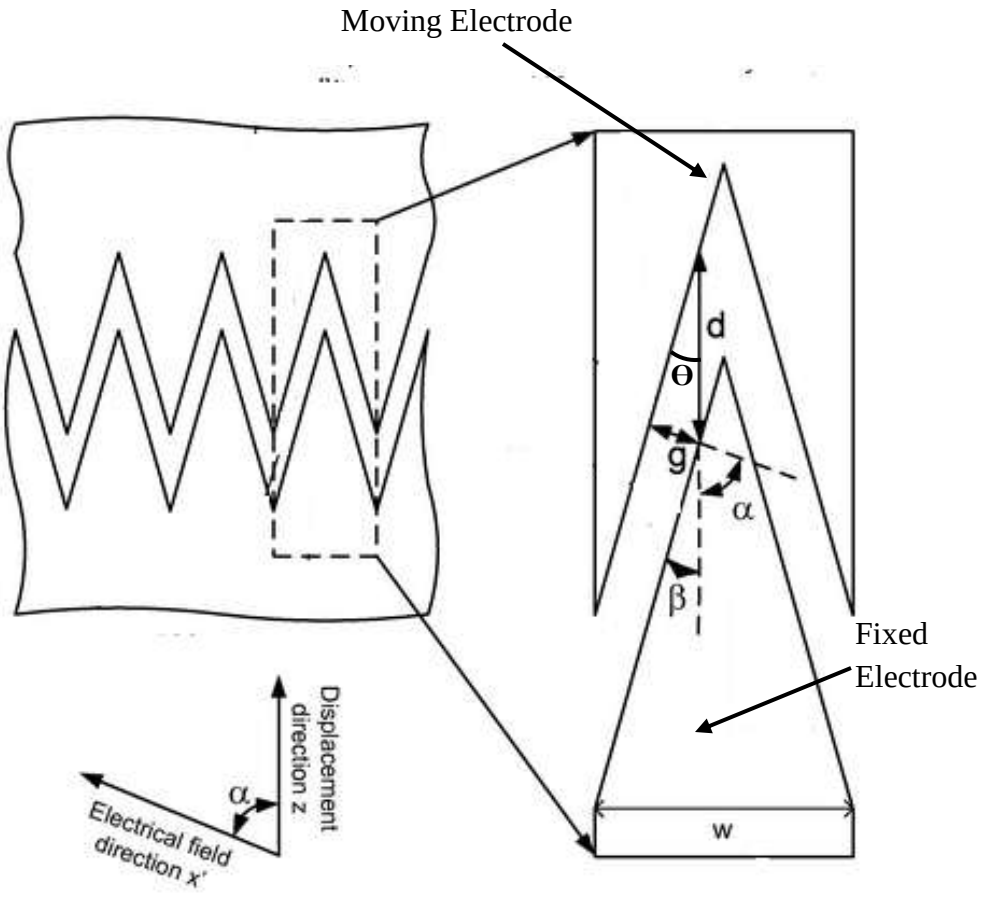

Figure 2.13: Standard saw tooth comb finger design for electrostatic force generation (Rosa et al., 1998)

The graph shown in Figure 2.14 clearly indicates the greater force generation capability of the device based on the use of angled comb fingers, displaying twice the achieved displacement of a counterpart device using rectangular comb fingers. This increase in force generation can be translated to other device optimizations including reduced operational voltage, decreased support beam length and a reduction in comb fingers, and hence an overall saving in device area. The added device stability provided by the shape of the angled (non-rectangular) comb finger is another important contribution to the enhancement of comb-drive micro actuator design.

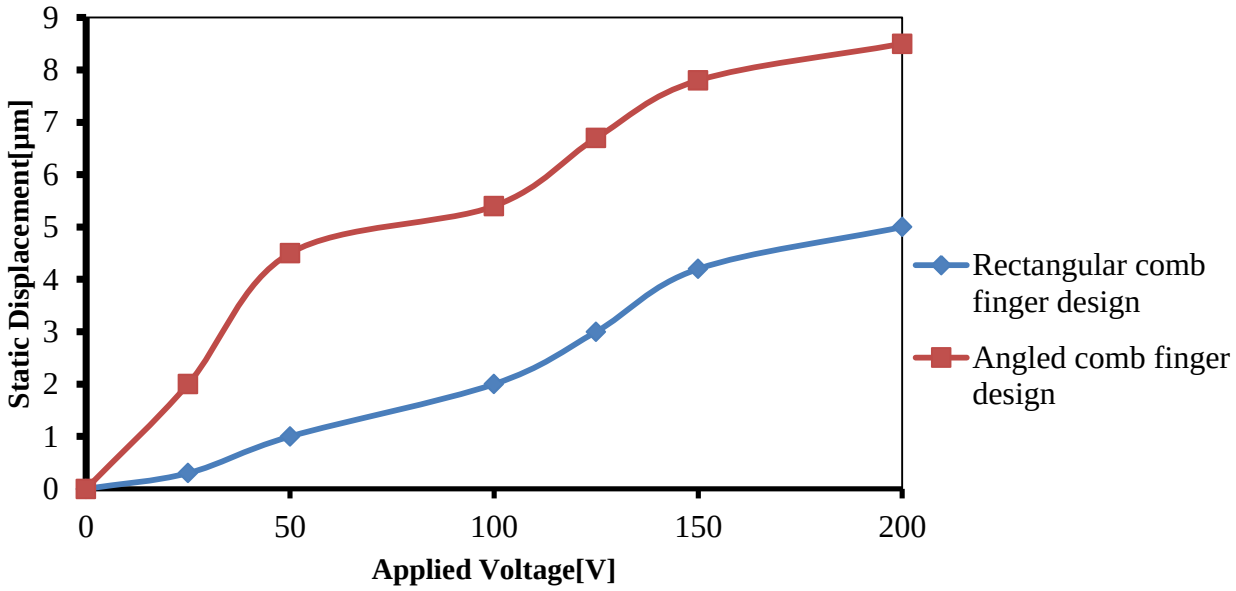

Figure 2.14: Measurements of static displacement for same applied voltage

(Rosa, Dimitrijev, & Harrison, 1998)

2.6 Spring

2.6.1 Spring type

The spring or flexure design for micro actuators is very important to support the actuator for a smooth actuation mechanism. Most micro actuators require spring design which have very flexible flexure design that deform in one direction, whilst having higher stiffness in the undesired direction for example the folded flexure design using in lateral resonator(Tang, Nguyen, Judy, & Howe, 1990). Most micro mechanical flexure or spring designs are created from straight beams.

From the work done by (Fedder, 1994), there are several types of common flexure design used for micro actuator in terms of fabrication method such as single beam flexure, crab leg flexure, folded beam flexure, and serpentine flexure. Figure 2.15 shows examples of flexure type and design. Distributed forces arising from weight of the beam, voltage between the beam and substrate and fixed charge in the substrate impose limitations on beam length. As the beam length is increased, these forces eventually cause the beam to touch the substrate (Fedder, 1994)

Cantilever guided end and fixed beams are shown in Figure 2.16 where a concentrated force F and a uniform distributed load f is applied to the cantilever. Axial displacement in Table 2.1 and Table 2.2 is found directly from Hooke's Law Lateral displacement equations are summarized where E is Young's modulus of elasticity.

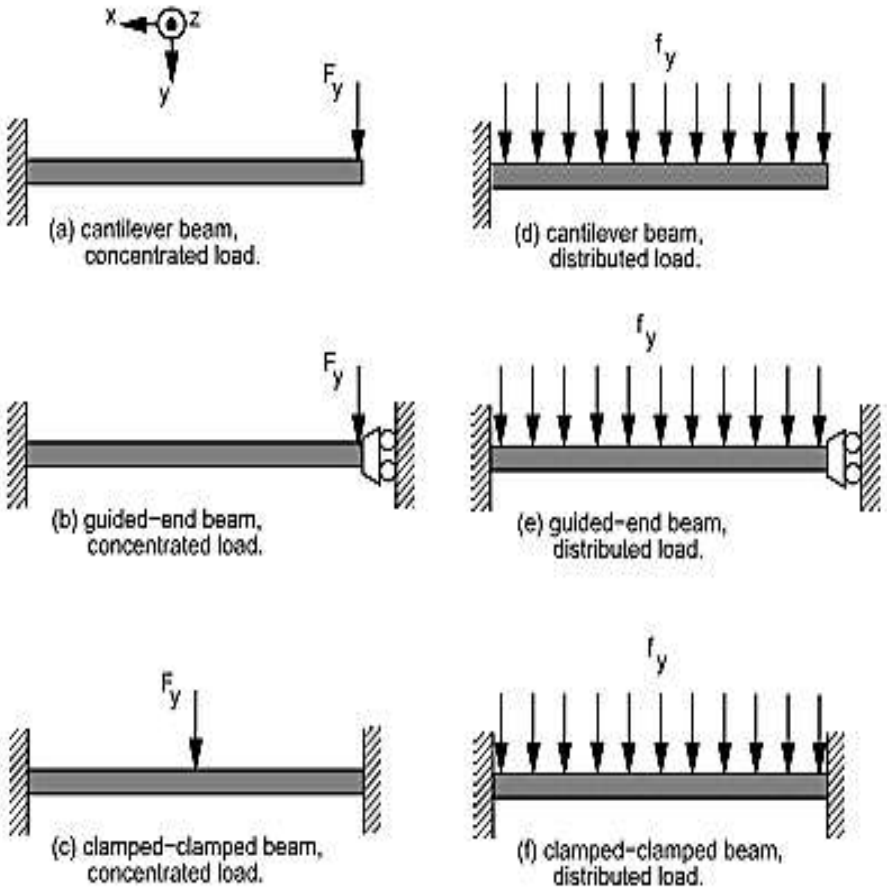

Figure 2.15: Various beams with concentrated load F (Fedder, 1994)

Table 2.1: Concentrated load

Cantilever	Guide-end	Fixed-fixed
$x = \frac{F_x L}{EhW}$	$x = \frac{F_x L}{EhW}$	$x = \frac{1}{4}\frac{F_x L}{EhW}$
$y = 4\frac{F_y L^3}{EhW^3}$	$y = \frac{F_y L^3}{EhW^3}$	$y = \frac{1}{16}\frac{F_y L^3}{EhW^3}$
$z = 4\frac{F_z L^3}{EWh^3}$	$z = \frac{F_z L^3}{EWh^3}$	$z = \frac{1}{16}\frac{F_z L^3}{EWh^3}$

(Fedder, 1994)

Table 2.2: Distributed load

Cantilever	Guide-end	Fixed-fixed
$x = \frac{f_x L}{E}$	$x = \frac{f_x L}{E}$	$x = \frac{f_x L}{4E}$
$y = \frac{3}{2}\frac{f_y L^4}{EhW^3}$	$y = \frac{1}{2}\frac{f_y L^4}{EhW^3}$	$y = \frac{1}{16}\frac{F_y L^3}{EhW^3}$
$z = \frac{3}{2}\frac{f_z L^4}{EWh^3}$	$z = \frac{1}{2}\frac{f_z L^4}{EWh^3}$	$z = \frac{1}{32}\frac{f_z L^4}{EWh^3}$

(Fedder, 1994)

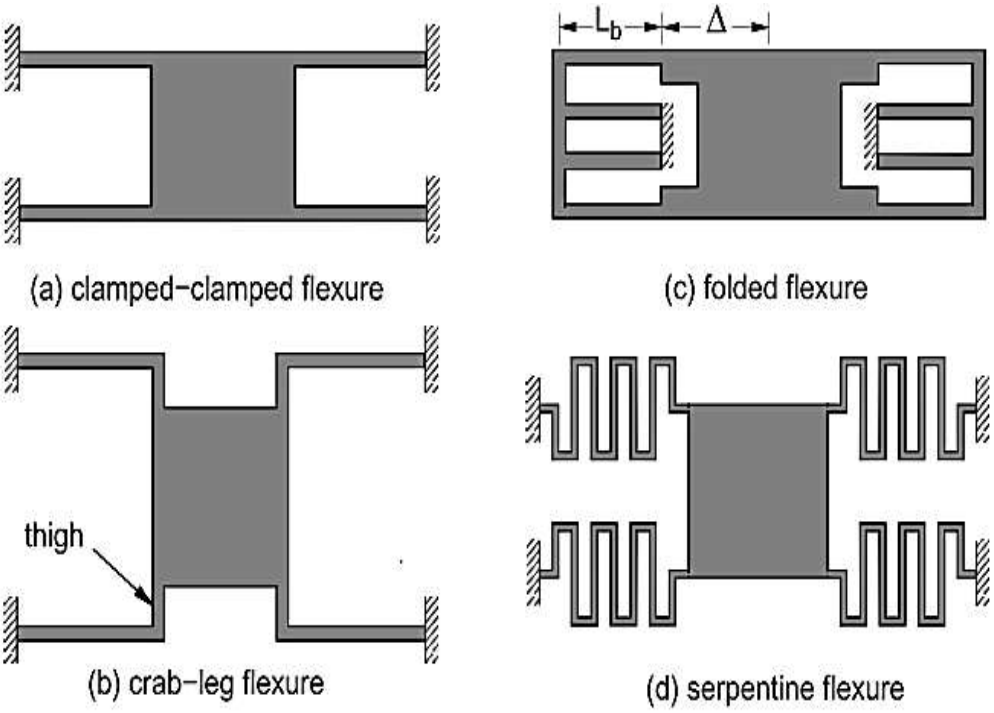

Figure 2.16: Various flexure designs (Fedder, 1994)

The serpentine spring type is one of spring designs used as flexure for comb drive actuators. It is an improvement from the crab-leg flexure, clamped-clamped flexure, and folded flexure. This type of spring can provide good linear behavior of displacement for the desired x-direction and simultaneously provide stiffness for undesired y-direction compared to the crab-leg flexure, clamped-clamped flexure, and folded flexure based on Fedder's studies. K is the mechanical stiffness of the spring, which is defined by

$$K = \frac{Et}{N}\left(\frac{w}{l}\right)^3 \qquad \text{(Equation 15)}$$

$$F = K\partial x \qquad \text{(Equation 16)}$$

Where E is Young's modulus, t is the thickness of the spring, N is the number of cantilever beams of the spring, w is the width of the beam, l is the length of the spring, F is mechanical force and ∂x is spring displacement. Figure 2.17 shows the serpentine spring used by (Tsay et al., 2005) for micro feeding application.

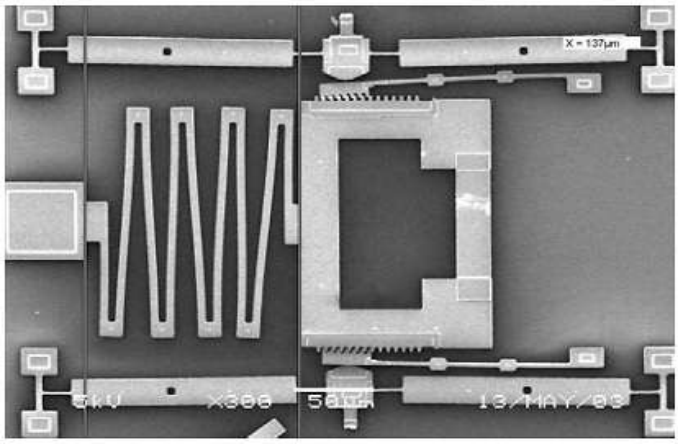

Figure2.17: Examples of serpentine spring used in microsystems (Tsay et al., 2005)

The serpentine flexure in Figure 2.18 is made of four serpentine springs. A schematic of a spring is shown in Figure 2.18. Serpentine springs beam segments shape like the meandering snake shape. Each meander is a of length and width b except for the first and last meanders which are of width c. The beam segments that span the meander width are called span beams or span. The beam segments that connect to the spans are called connector beams or connector. In some spring design, the width of the first and last meanders is half that of the other meanders. Because of the flexure the end of the spring has a guided end boundary condition where only motion in the preferred direction is allowed (Fedder, 1994).

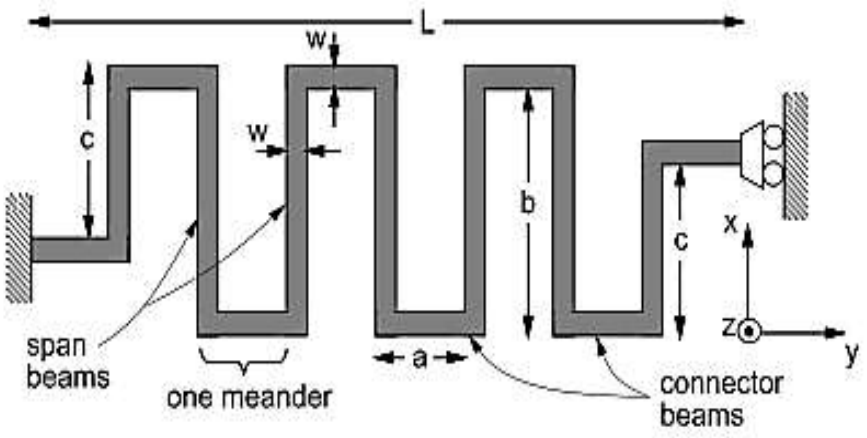

Figure 2.18: Examples of serpentine spring used in microsystems (Fedder, 1994)

2.8 Electrostatic Comb Drive Micro Actuator Applications

2.8.1 Micro resonator

Micro resonators are structures which are not designed to produce linear translation, but to vibrate. It can be used to replace electronic resonators, being used in electronic filter systems. This is highly used in telecommunications. For example, in mobile phone communication, each telephone uses a precise frequency included in a range, depending on the protocol. The filter must keep only the chosen frequency, so that the system cannot be interfered by other people's conversations during the calls. All mechanical systems have specific resonance frequencies (Kalicinski, Tilman, Wevers & De Wolf, 2009) (Lagouge, 2009).

The micro resonators use mechanical vibrating parts to filter signals so that only one frequency, the Eigen frequency of the structure, is kept. The application is for electronic signal treatment, so, there must be a way to convert electrical signal into mechanical stimulation, and then back again for mechanical vibration into an electrical signal, based on the principle of electrostatic (Kalicinski, Tilman, Wevers & De Wolf, 2009).

The vibrating part includes as well the electrode for stimulation, and the electrode for measurement. Then, a lot of architectures are under studies in research laboratories, including different shapes and electrodes configuration for mechanical and electrical parts.

The vibration was formed by the incoming electrical signal. Then, the amplitude of the vibration depends on how close the input frequency is to the Eigen value. On the output, a polarization (constant voltage) between the resonator and the output electrode allows the measurement of the amplitude of vibration. Since the amplitude difference obtained between the Eigen frequency and other ones are very high, the electrical output signal for

any non-selected frequency is considered as neglected, whilst the Eigen frequency signal is kept (Lagouge, 2009).

Figure 2.19 shows an example of micro resonators architectures, which correspond to Intermediate Frequencies (IF). Intermediate frequencies are a convenient way of treating a signal between low frequency (the human voice frequency) and really high frequencies (at which mobile phones communicate).

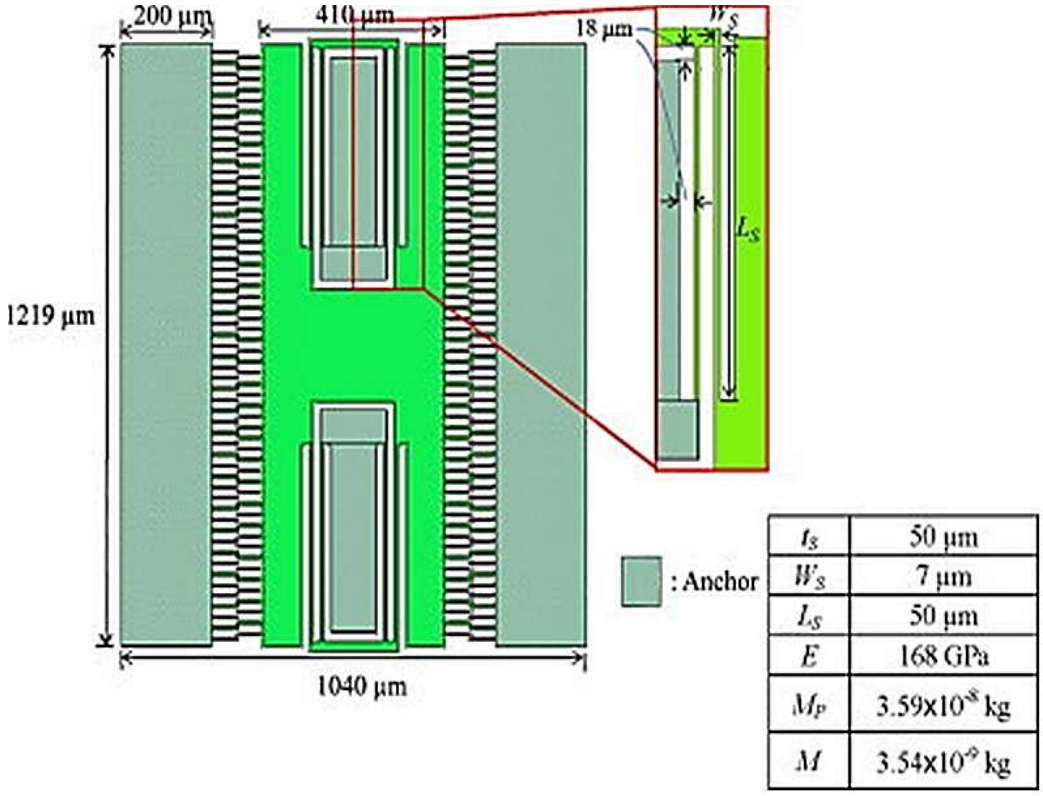

t_S	50 µm
W_S	7 µm
L_S	50 µm
E	168 GPa
M_P	3.59×10^{-8} kg
M	3.54×10^{-9} kg

Figure 2.19: Example of micro resonator (Park, Kim, Jeong, Song & Kim, 2011)

2.8.2 Micro gripper

The basic operation of the micro gripper is based on the principle of the comb driver which comprises of an array of interdigitated comb fingers, where one set is fixed to the substrate and the other one is free and movable connected to a spring (Volland, Heerlein & Rangelow, 2002). The fundamental performance of the micro-gripper or micro-tweezers is that it relies on its ability to firmly hold objects with a high force density (Wang, Shen & Chen, 2015). However, high precision of force control is also required in order to maintain the grip of the object without damaging the material (Defeng, 2008). Figure 2.20 show example of electrostatic comb drive used in micro gripper systems proposed by (Dafflon, Lorent, Clavel, Beyeler & Nelso, 2006).

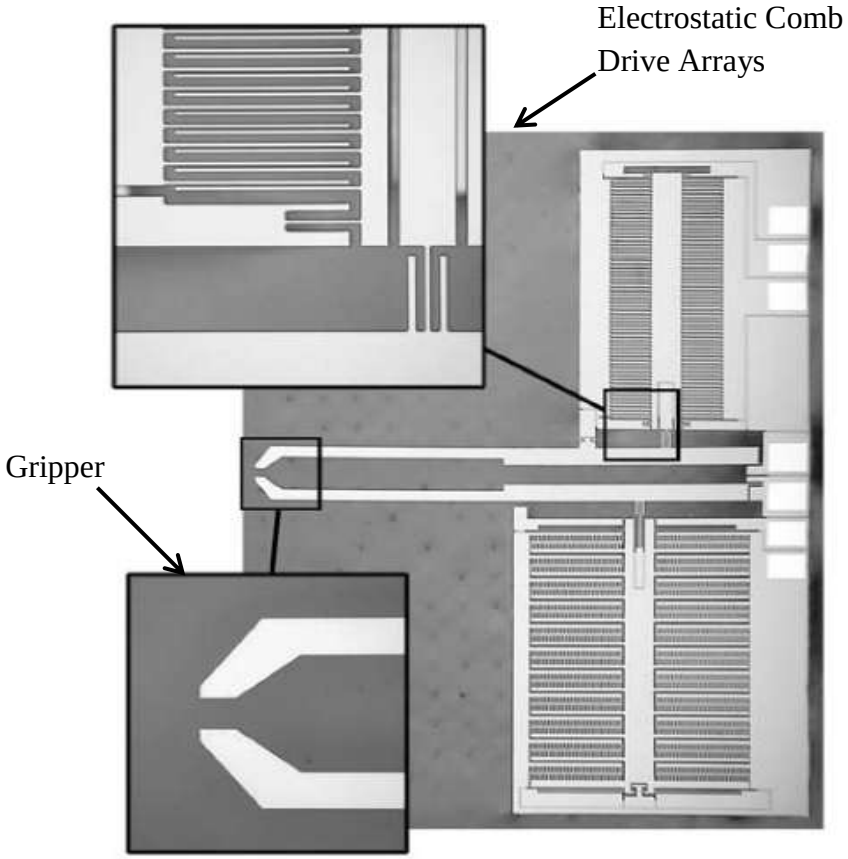

Figure 2.20: Example of electrostatic comb drive micro gripper systems

(Dafflon, Lorent, Clavel, Beyeler & Nelso, 2006)

2.9 Multiphysics Simulations Software Used

In this study, COMSOL Multiphysics version 4.3 is used for coupled analysis because of the interactive and user friendly for modeling and meshing. COMSOL Multiphysics is a powerful interactive environment for modeling and solving all kinds of scientific and engineering problems (Multiphysics, 2012). The software provides a powerful integrated desktop environment with a Model Builder where a full overview of the model and access to all functionality can be obtained. With COMSOL Multiphysics, extend from conventional models can be done easily for one type of physics into multiphysics models that solve coupled physics phenomena and do so simultaneously. When solving the models, COMSOL Multiphysics uses the proven finite element method (FEM). The software runs the finite element analysis together with adaptive meshing and error control using a variety of numerical solvers (Multiphysics, 2012). The studies can make use of multiprocessor systems and cluster computing, and can run batch jobs and parametric sweeps. COMSOL Multiphysics creates sequences to record all steps that create the geometry, mesh, studies and solver settings, and visualization and results presentation (Comsol, 2005). It is therefore easy to parameterize any part of the model and simply change a node in the model tree and re-run the sequences. The program remembers and reapplies all other information and data in the model (Multiphysics, 2012).

CHAPTER 3

RESEARCH METHODOLOGY

As shown in Figure 4.1, the electric field was modeled after structural to calculate the electrostatic force using steady state analysis which involves meshing only on the surrounding of the dielectric area of the fixed and moving electrode. In this case, COMSOL are used as simulation tools to simulate electric field. Then, dynamic modeling are modeled for mechanical where comb drive actuator including spring design are modeled and meshed to calculate displacement output based on electrostatic force calculated previously which will be applied as comb drive actuator load input.

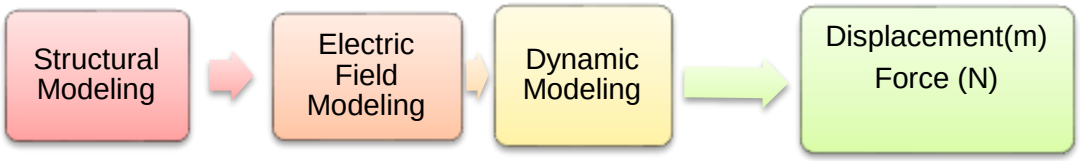

Figure 3.1: Methodology

3.1 Software Used

COMSOL 4.3 is used for modeling and optimization where modules used are Electrostatic module (structural and electric field modeling), Solid mechanics module (structural and dynamic modeling) and Moving mesh module (structural and dynamic modeling).

3.2 Numerical Analysis and Finite Element Methodology

In order to evaluate the performance of the actuator, finite element analysis was conducted using COMSOL Multiphysics. The objectives of this simulation are to predict the actuator displacement and force for both a conventional straight sided electrostatic comb actuator and the fishbone shaped actuator in this design. First, simulation of a single finger of the straight sided actuator and fishbone shaped actuator were performed, and their performances were compared. Next, simulation of an array of straight sided and fishbone shaped actuators was performed, for a fixed active area for the two cases in order to compare the performance of the two types of electrostatic comb actuators.

The simulation was chosen to be in 2D as the main investigation for this paper is the translational force and displacement in the XY plane. The model applies an electric potential for the moving electrode and grounded the fixed electrode.

The electrostatic comb driver is capacitive device where the electrostatic problem at hand is represented by Laplace's equations to find potential distribution (**V**) of the geometry.

$$\nabla^2 V = \frac{\partial V^2}{\partial X^2} + \frac{\partial V^2}{\partial Y^2} = 0 \qquad \text{(Equation 16)}$$

The electric energy $\mathbf{W_e}$ and capacitance **C** are solved for all element nodes, based on

$$\boldsymbol{W_e = \frac{1}{2}\varepsilon_0 \iint |E|^2 dxdy} \quad \text{(Equation 17)}$$

$$\boldsymbol{C_t = \frac{2}{V^2}\iint W_e dxdy} \quad \text{(Equation 18)}$$

Where C_t is the capacitance per unit thickness,

The electrostatic force between comb fingers is related to the voltage and capacitance changes, as the physical motion of the actuator continuously induce a change in the spacing and overlap, which has a direct impact on the values of capacitance and voltage. The relationship between electrostatic force $\mathbf{F}_{es}$ is related to the rate of change of the electrostatic energy in the direction of motion (x), and consequently related to the rate of change of capacitance in the x direction (for a fixed voltage) as shown below, where

$$\mathbf{F}_{es} = -\frac{\partial W_e}{\partial x} = \frac{\partial C(x)}{\partial x} \cdot \frac{V^2}{2} \quad \text{(Equation 19)}$$

Where $\mathbf{W_e}$ is electric energy, and $\mathbf{F}_{es}$ is the electrostatic force.

3.3 COMSOL Simulation Steps

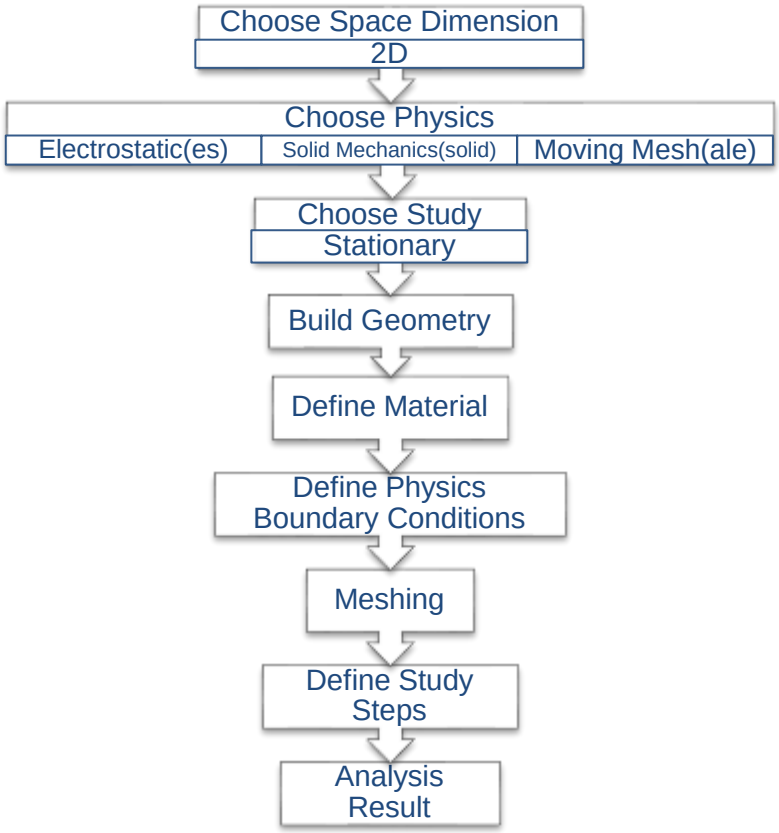

Figure 3.2: COMSOL simulation steps

3.3.1 Choose Space Dimension

First step for simulating using COMSOL is to define space dimension to be 2D analysis as shown in Figure 3.3. For the electrostatic case, 2D analysis can minimize the computer memory consumption and reduce computational time by reducing number of element meshing. From (Harouche & Shafai, 2005) work, 2D analysis is good enough to show comparison of the electrostatic profile of the comb drive actuator design.

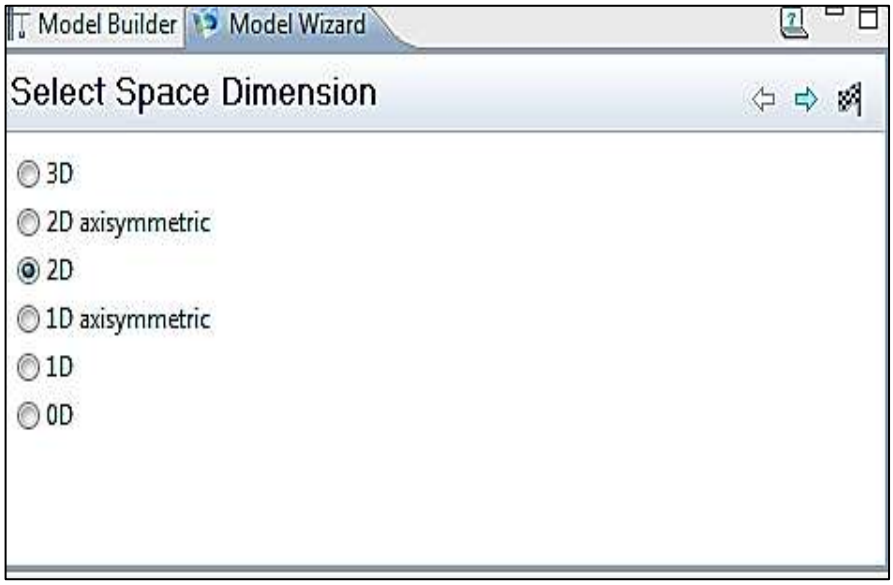

Figure 3.3: Space dimension selection

3.3.2 Add physics

The second step is adding the governing equation involve in the simulation process. The physics module used was electrostatic in AC/DC module for simulating electrostatic force and that had been added is solid mechanics in the structural mechanical module. The drive force data from electrostatic analyses are coupled with solid mechanics analysis as boundary load input to simulate the displacement of the comb drive actuator. Solid mechanics was also coupled with moving mesh physics to show deformation of the comb driver caused by electrostatic actuation.

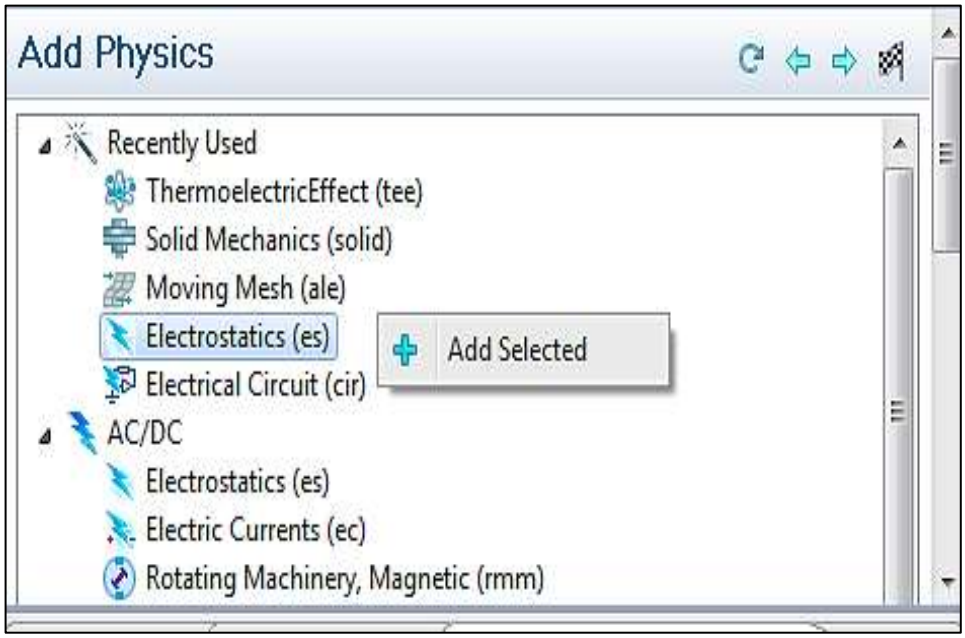

Figure 3.4: Physics selection interface

3.3.3 Geometry modeling

Geometry modeling as shown in Figure 4.5 was carried out in the X-Y plane because of 2D space dimension selection in the previous step. Geometry modeling for this study involved a two parts of modeling process. First the electrode was modeled and the second is the dielectric area surrounding the conductor.

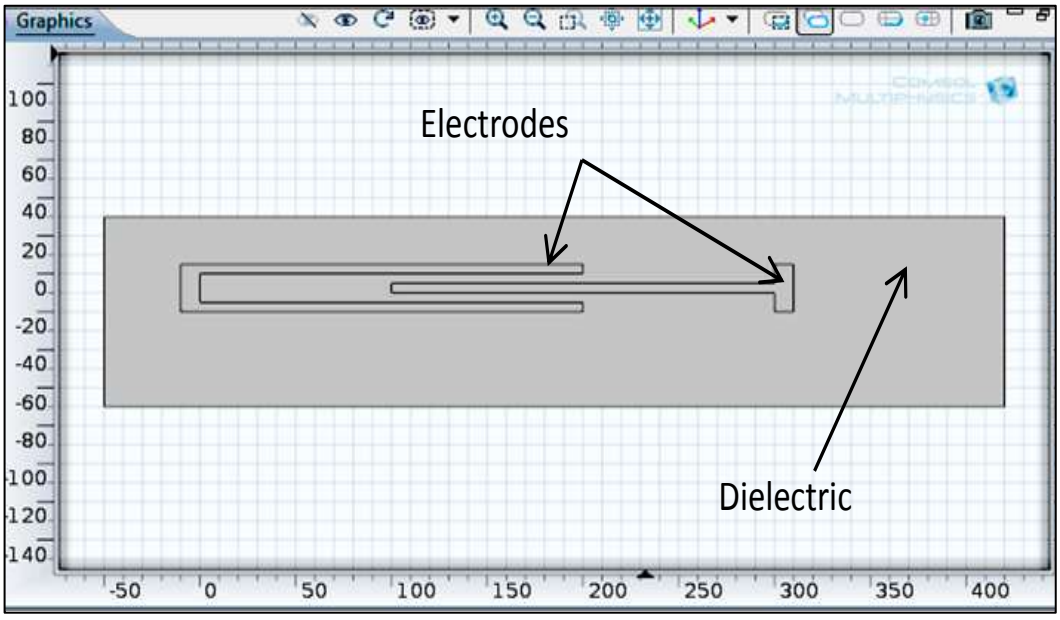

Figure 3.5: Example of geometry modeling

3.3.4 Choose Study

In this study, the study type was defined as stationary where the electrostatic analysis and structural mechanical analysis were done in steady state analysis.

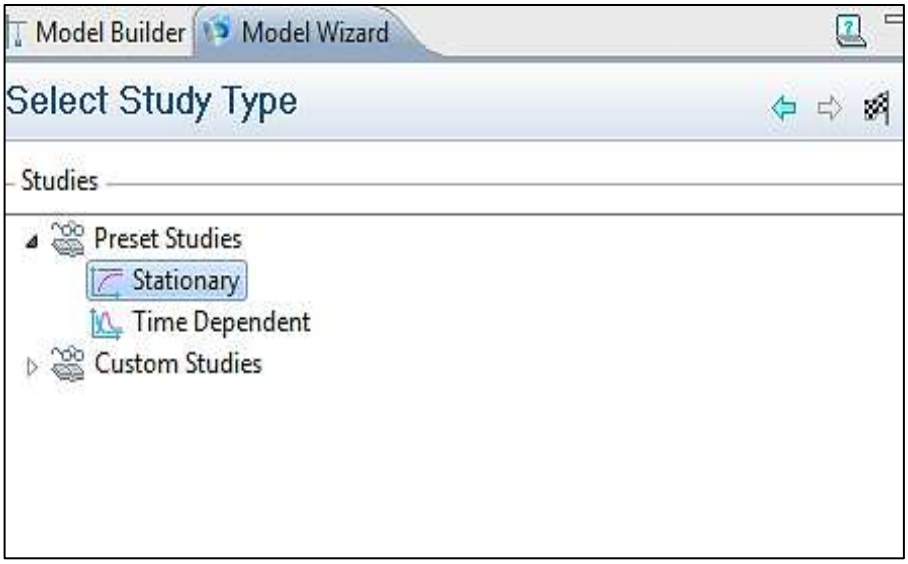

Figure 3.6: Study type selection interface

3.3.5 Define material

There are two parts of material definitions involved in the simulation. First, the fixed electrode and moving electrode were defined as silicon where the relative permittivity is 11.7, Poisson's ratio is 0.28, Young's modulus is 170e-9 Pa and density is 2329 kg/m3. The second part is defined as the surrounding of the conductor as air for dielectric area where the relative permittivity is 1.

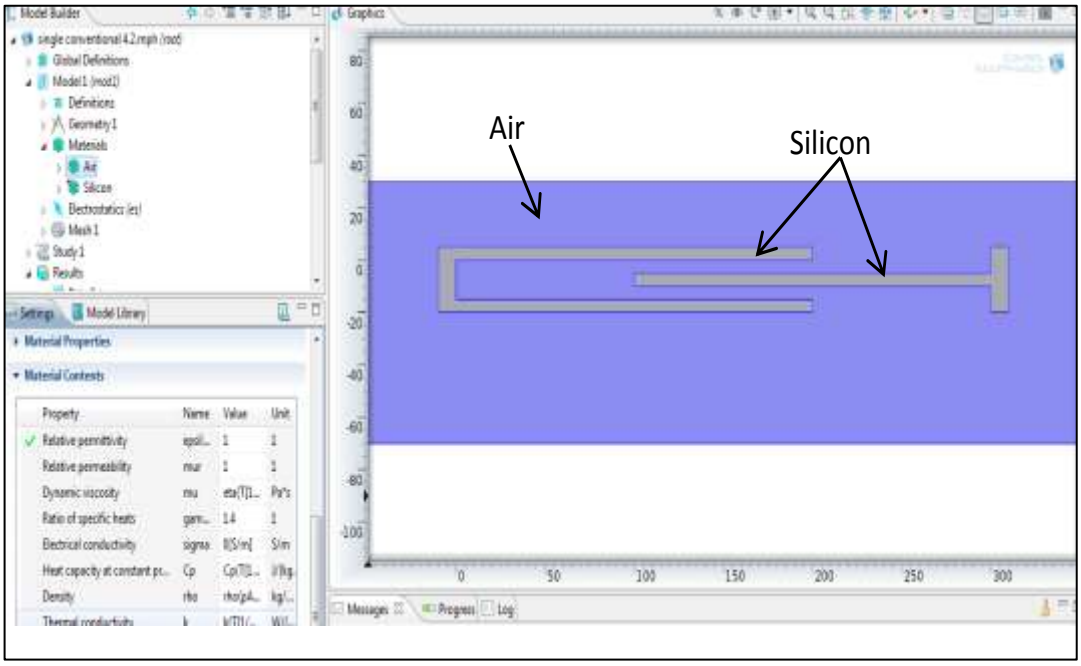

Figure 3.7: Example of material definition for dielectric area

3.3.6 Define load

After defining the material for the model, boundary conditions were defined based on the physics and analysis. For electrostatic analysis, the boundary condition for fixed electrode was defined as ground and the moving electrode was applied with electric potential ranging from 0-100 Volt. Then, for the structural mechanical analysis, the boundary condition for fixed electrode was defined to be fixed, and the moving electrode was applied with drive force that was coupled from the electrostatic analysis which drives the translation of the comb drive actuator. Then, for the moving mesh physics, the boundary conditions for fixed electrode was defined to be fixed mesh and for moving electrode and the dielectric area, the boundary conditions were define to be free deformation.

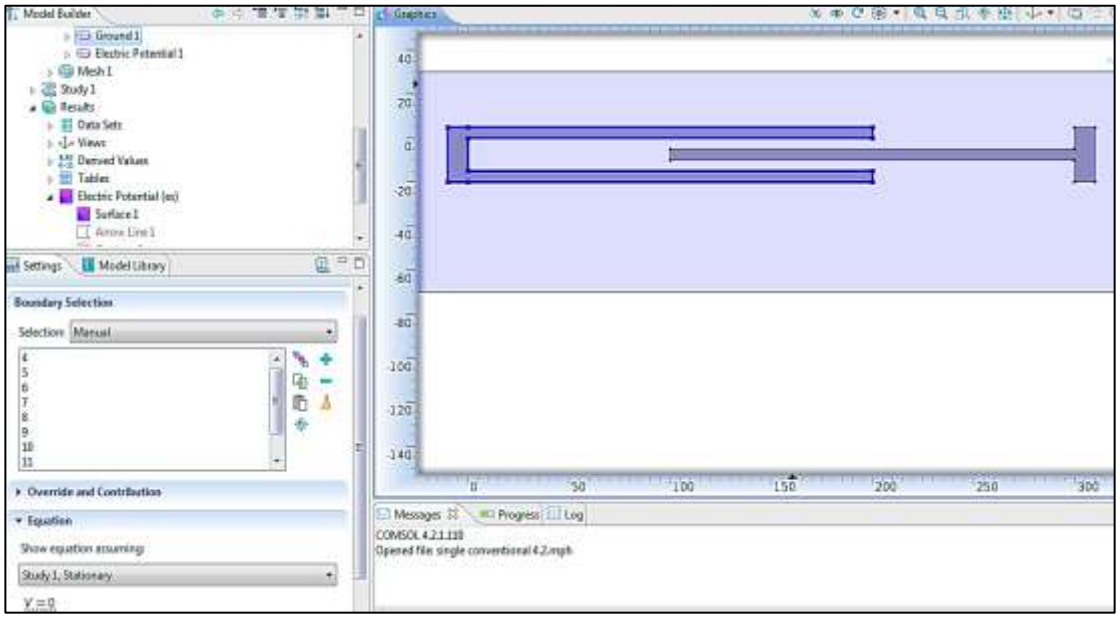

Figure 3.8: Example of boundary condition selection

3.3.7 Meshing

The meshing process easily been carried out using COMSOL, where the meshing process can be carried out simultaneously for multiple analyses and automatically generated. Based on (Harouche & Shafai, 2005), the quadratic element was chosen for the meshing element type because the quadratic element resulted faster convergence and high accuracy rather than using linear element. Meshing was automatically generated using the triangular mesh shape. From (Harouche & Shafai, 2005), after 5000-7000 numbers of elements without extra refinement, the results begin to convergence as shown in Figure 3.9.

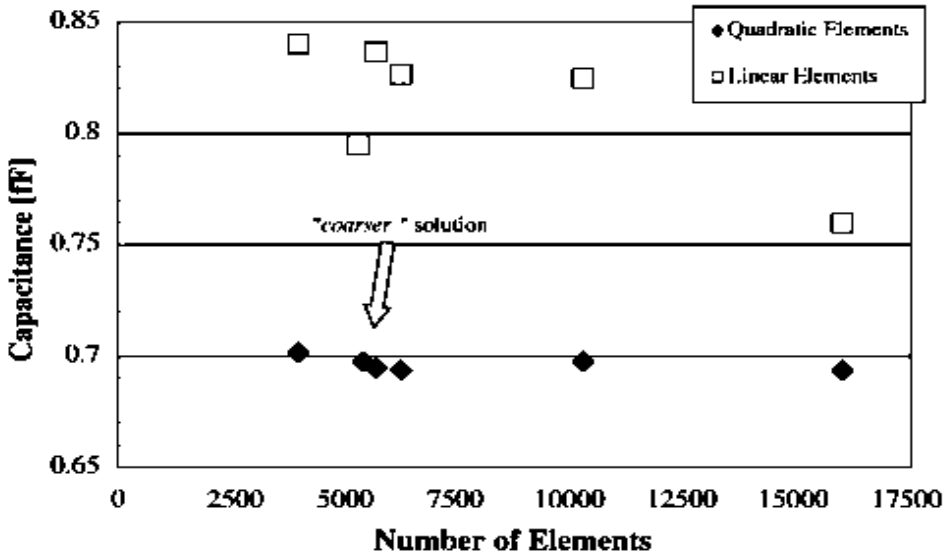

Figure 3.9: Mesh studies (Harouche & Shafai, 2005)

3.3.8 Define study steps and solver

Study steps were defined based on the parameter ranges which in this study, all models were analyzed based on the variation in electric potential variations range from 0-100 Volts and the step size was defined as 10 Volts. The solver for this study was defined to be non-linear because of the non-linear geometry shape order and quadratic elements used in meshing in the simulations.

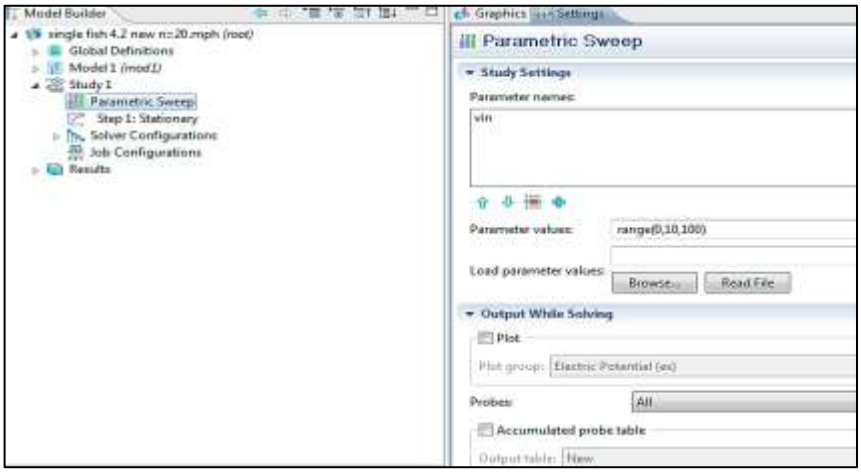

Figure 3.10: Study step definition process in COMSOL

3.3.9 Analysis of results

Analyses were carried out based on the simulation result. From electrostatics analysis, the electric field distributions was plotted to observe the characteristics of the electric field profile for the model after application different electric potential to the electrodes. Comparisons of electric field distributions have been carried out for conventional electrostatic comb drive actuators with fish bone shaped comb driver. Then electrostatic forces were plotted and compared for both the conventional comb drive and fish bone shaped comb driver before being fed in as input for the structural mechanical analysis. From coupled analysis of the electrostatic results with the structural mechanical results, the displacements of the actuator were plotted. Deformation of the actuator may be observed by coupled the structural analysis with moving mesh physic to allow deformation for the actuator and large displacement study as shown in Figure 3.11.

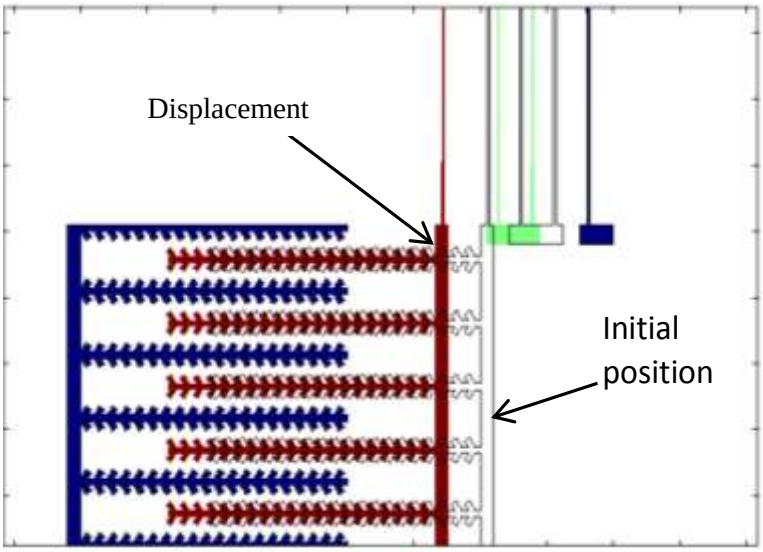

Figure 3.11: Example illustration of the actuator deformation through the use of a moving mesh module

3.4 Optimization Simulation Step of Fish Bone Shaped Comb Drive Actuator Using Comsol

Electrostatic force is simulated using electrostatic analysis in AC/DC module in COMSOL. From electrostatic analysis, electric field distribution and drive force data were simulated. The drive force data than is used as input for coupled analysis of electrostatic analysis with structural mechanical analysis in solid mechanics module in COMSOL to simulate the displacement of the actuator. For the structural analysis, the electrostatic comb fingers were merged with spring design to form electrostatic actuator mechanism where the actuation is caused by the drive force produced by the electrodes and the displacement are depend on spring stiffness. The drive force performance and displacement performance of fish bone shaped comb driver are compared with the performance of the conventional comb driver where optimizing need to be done again when drive force of the conventional comb driver is larger than fish bone shaped comb driver.

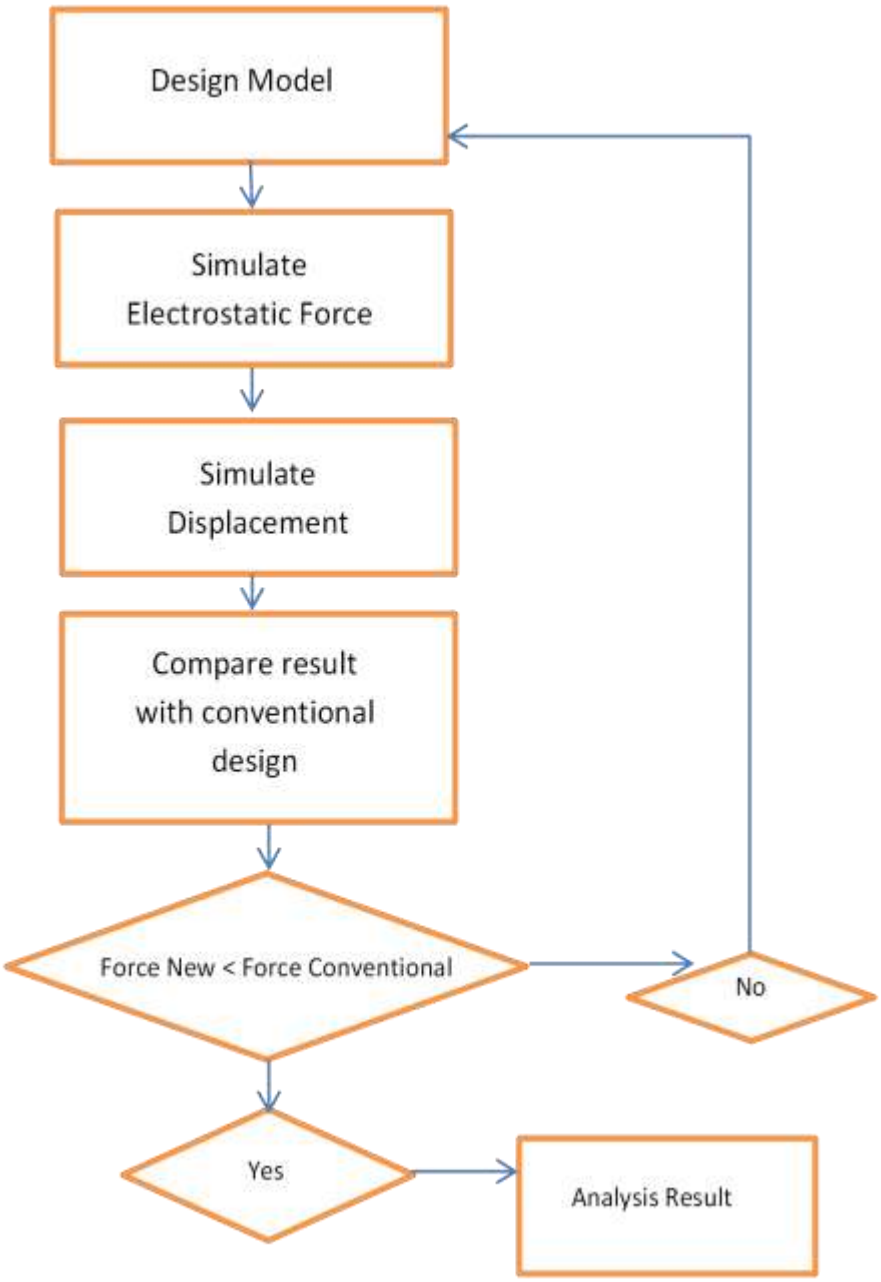

Figure 3.12: Optimization step

3.5 Design Concept

3.5.1 Conceptual design of fishbone shape electrostatic comb drive actuator

The design of the fishbone-shaped electrostatic actuator is shown in Figure 3.1**,** which is intended as a high force density actuator due to the interdigitated fishbone profile. The electrodes are made of silicon. In this Figure 3.13, a single finger acts as a backbone from which a series of smaller fingers protrude, twenty five in this particular illustration. The magnified section shows the labeling of the respective dimensions for the fishbone structure. The center electrode is allowed to be movable, whilst the upper and lower electrodes are fixed. A minimum gap defined as *g* was set to 3μm. The width of the central backbone of the fixed electrode is defined as *w*. The overall comb design achieves a fishbone look, where small fingers are attached at an angle to the backbone electrode, for both the fixed and moving electrodes. There are constant separations between arrays of small protruding fingers connected within the electrode defined, as *r* which lead to an increase in the capacitance of the comb driver as a result increase the force density. However, the value of *r* will affect the number of small fingers *N* that can be connected within the electrode which large value of *r* will decrease the number of protruding small fingers that can be connected to the electrode**.** The effect of *r* to the force generated by the actuator is analyzed for this study**.** The number of interdigitated small fingers, *N* within the electrode expected to affect the magnitude of force generated by the actuator**.** The parameters of *a, b,* c and *d* collectively define the angle **θ°** relative to the position of the electrode is as shown in Figure 3.14. These small fingers are placed at an angle **θ°** to the backbone and face each other inwards whilst interdigitating between fixed and moving electrodes. For the small finger protrusion, several combinations for parameters *a, b, c* and *d* were selected, which produced certain discrete values of the angle **θ°.** For this study, the

minimum dimension for the parameters of *a*, *b*, *c* and *d* was defined as 3µm, and the effect of the angle **ɵ°** to the force generated by the comb driver was analyzed**.** This angled small finger yielded resultant electrostatic fields which possessed components in both the X and Y direction. Whilst the forces in the Y-direction cancel out due to symmetry, the superposition of the resultant force in the X-direction add up to form a strong driving force in the X-direction. This increase of force in the X-direction is due to the fishbone geometry.

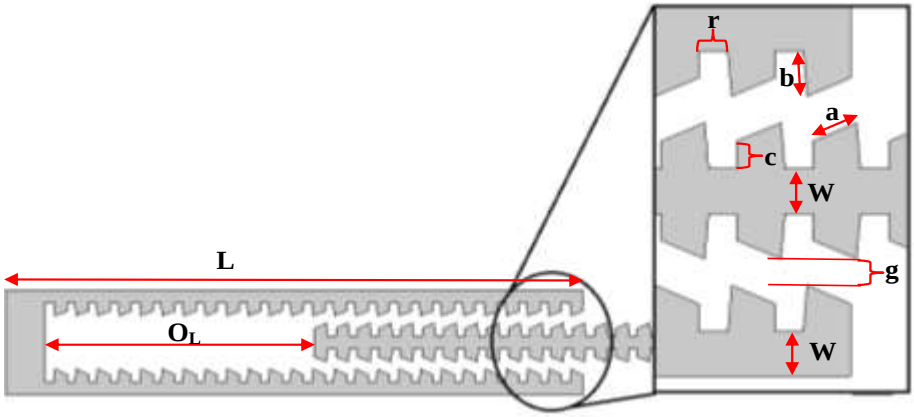

Figure 3.13: Example of a single finger of fishbone shaped comb driver

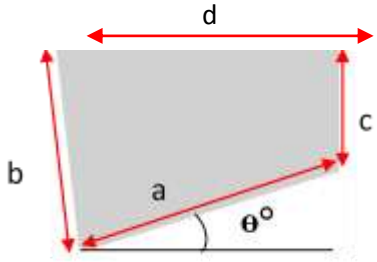

Figure 3.14: Example of small fingers placed at an angle ɵ° relative to the electrode

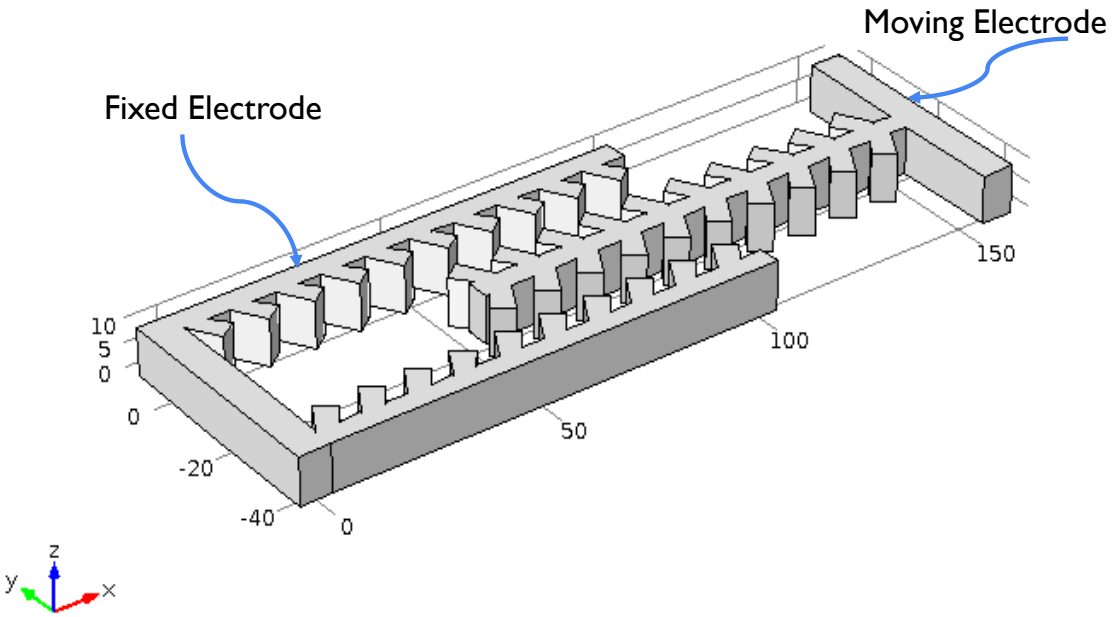

Figure 3.15: Example of single finger fish bone shaped comb drive actuator

A spring component was built into the actuator design to provide restraining force and flexibility to the actuator motion as shown in Figure 3.16 where $K_{m\,is}$ spring stiffness.

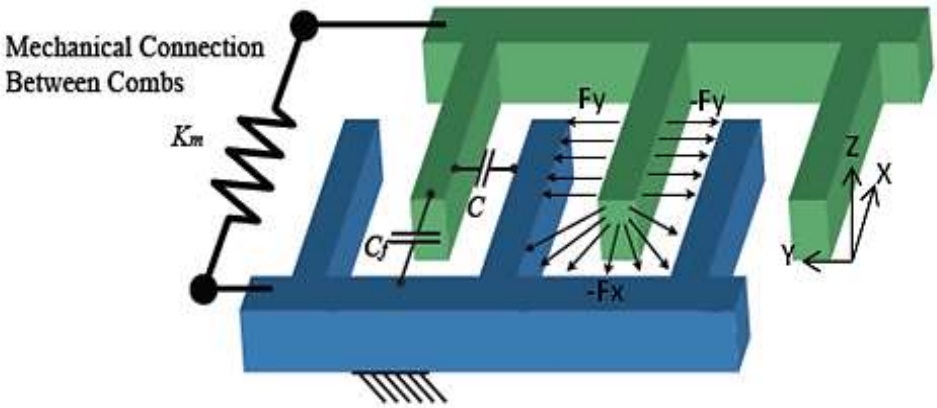

Figure 3.16: Example of conventional comb drive actuator system

The serpentine spring type was selected for both designs of comb drive actuators for actuation and deformations studies, as it in particular provides good restraining force against the electrostatic force acting in the y direction, which is a main cause of instability. The close up of this serpentine spring can be seen in Figure 3.17.

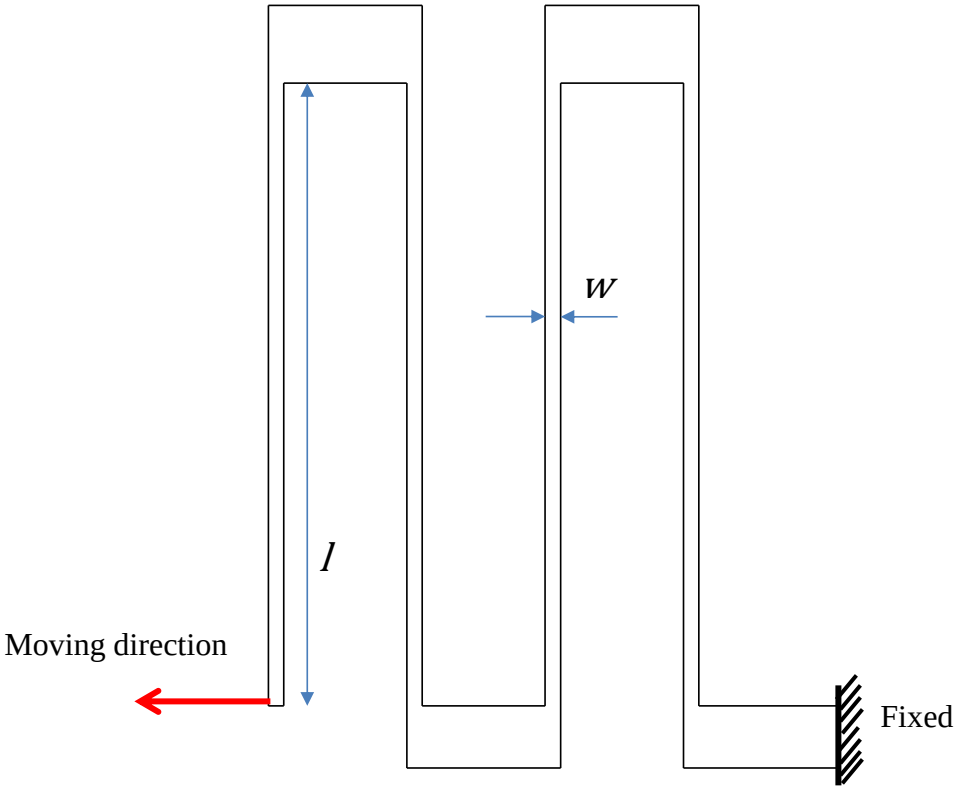

Figure 3.17: A close up of the serpentine spring used in the simulation

This type of spring can provide good linear behavior of displacement for the desired x-direction and simultaneously provide stiffness for undesired translation in the y-direction. **K** is the mechanical stiffness of the spring, which is defined by (Tsay, Su & Sung, 2005).

$$\mathbf{K} = \frac{Et}{N}\left(\frac{w}{l}\right)^3 \qquad \text{(Equation 20)}$$

$$\mathbf{F} = K\Delta x \qquad \text{(Equation 21)}$$

Where *E* is young modulus, t is thickness of the spring, *N* is the number of cantilever beams of the spring, *w* is width of the beam, *l* is the length of the spring, **F** is mechanical force and

Δx is spring displacement. All the parameters of the spring below were used in the equation (3) and the theoretical value for a serpentine spring using parameters defined in Table 3.1 is 0.034 N/m.

Table 3.1.Parameters of spring design

Parameters	Values
Young's Modulus , *E*	1.70 x 10^{11} Pa
Thickness, *t*	100 µm
Number of cantilever beams, *N*	4
Width, *w*	2 µm
Length, *l*	1000 µm

However, for this design geometry, a cogging effect, which is a periodic variation of its force-displacement profile, is anticipated. This is due to the component of electrostatic force from each minimum gap (g), which results in a translational motion in the negative direction from each these gaps. Thus, a strategy to overcome this cogging effect is required to ensure smooth translational motion.

A suggested strategy to mitigate this cogging would be the "finger shifting method". A finger shifting value $F_s(n)$, in µm, can be expressed as follows:

$$F_s(n) = \left(\frac{p}{s}\right) n \qquad \text{(Equation 22)}$$

For n=[0, 1, 2, 3….,n_{max}].

Where, $F_s(n)$ is the finger shifting value for the nth position of comb finger, s is the step size factor (s≠0), p is the pitch of the small protrusion, i.e. the distance between two teeth, and n_{max}=s-1. F_s cannot be defined to be negative to maintain the minimum overlap for the actuator motion. The definition for p (in µm) is illustrated in Figure 3.6 as described below:

$$p = r + d \qquad \text{(Equation 23)}$$

where r is the figure spacing and d is the figure thickness.

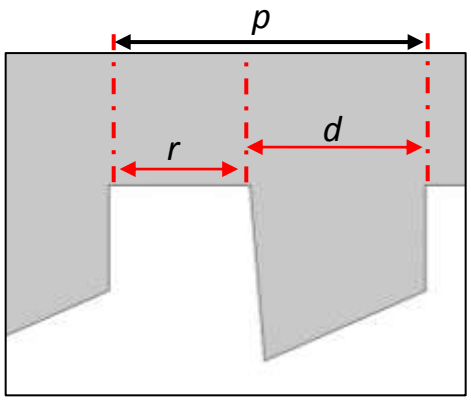

Figure 3.18: The position of p in fish bone shape comb driver

The value of s cannot be negative to maintain the minimum overlap for the actuator motion where s= [1, 2, 3, ...∞].

Geometrically, referring to the position of the electrode in Figure 3.7, electrode (1) is fixed, whilst electrodes (2), (3), (4), (5), (6) and (7) are defined by finger shifting value $F_s(n)$. The effect of this finger shifting on the overall displacement profile of the moving electrode is through the principle of superposition, where the minimum points of displacement are expected to cancel out.

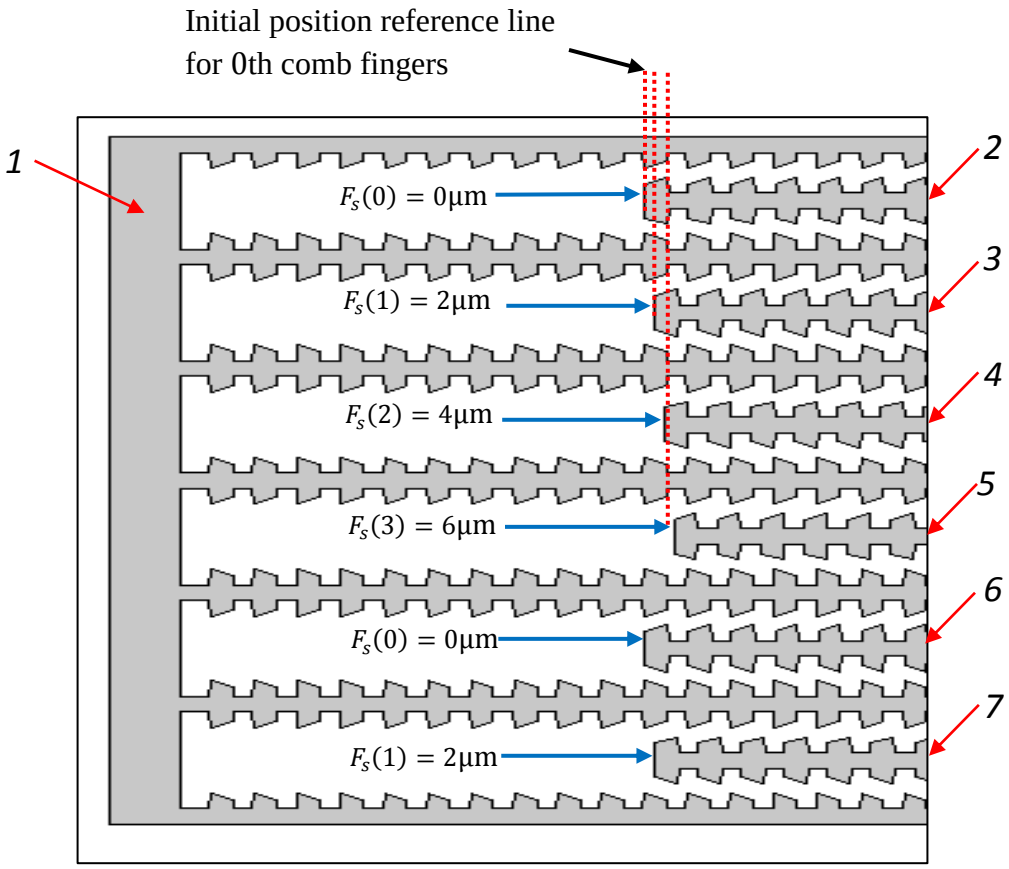

Fig. 3.19: Example of finger shifting method applied to six comb fingers of fishbone shaped comb driver array with $n_{max} = 3$, $F_s(n) = 2n$ (μm), $n = [0, 1, 2, 3, 0, 1, 2, 3]$, m =6 comb fingers, $p = 8$ μm

3.5.2 Multiple fingers with almost same cross sectional area

Cross sectional area for single finger of conventional comb driver and single finger of fish bone shaped comb drive actuator are different where fish bone shaped comb drive actuator consume more cross sectional area than conventional comb driver. For the force density comparisons, both designs are remodeled for multiple fingers with almost same cross sectional area. However, for this study, the number of fingers are designed limited to 16 fingers for fish bone shaped comb drive actuator and 40 fingers for conventional comb driver with cross sectional area 800 x 300 µm because of computer memory and processor limitations. Multiple fingers of electrostatic comb drive actuator analysis are easily done using COMSOL where all analysis can be done simultaneously which conserve more computational and modeling times.

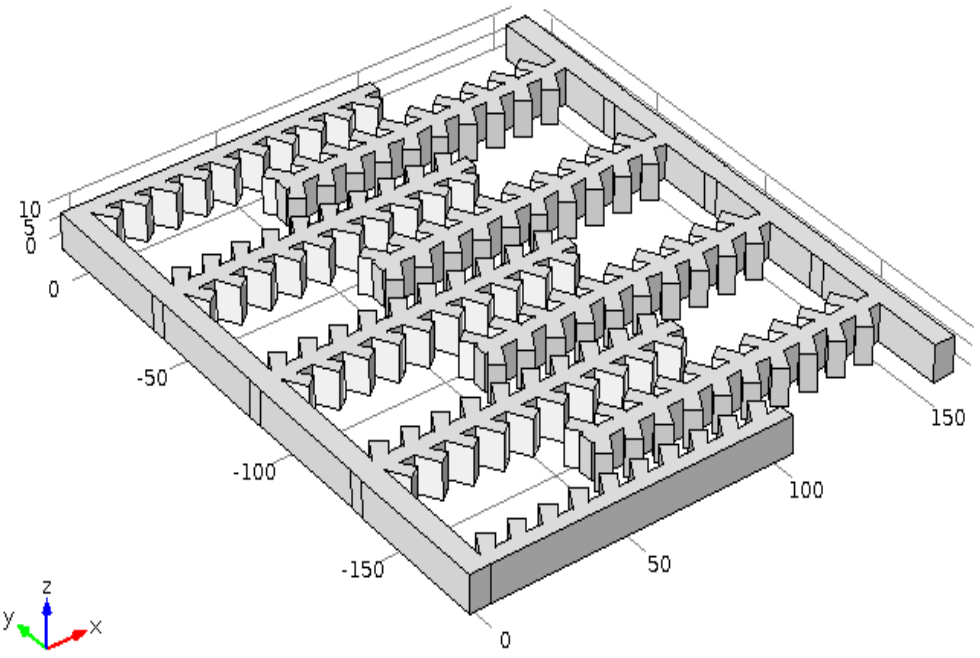

Figure 3.20: Example of four multiple fingers of fish bone shaped comb drive actuator

CHAPTER 4

RESULTS AND DISCUSSION

4.1 Meshing Stability Analysis

A simple mesh refinement study was performed in order to identify the optimal mesh size. The boundary element mesh consisted of triangular elements generated using COMSOL tools. The conventional straight sided electrostatic actuator was simulated using a wide variety of mesh parameters, which produced a large range for the number of elements produced in each mesh. The capacitance and electrostatic force acting in the moving finger was simulated for each mesh. Figure 4.1 show the percentage difference in the predicted force compared to that predicted by the finest mesh. Based on this procedure, the mesh size which yield as compromise between computational effort and accuracy of calculation was chosen. For this study, the number of elements after the meshing process is about 10000, which includes the extra refinement at the edge of the models. Figure 4.2 give an example of the meshing results for a single finger of fish-bone shaped comb drive actuator contains 10000 elements.

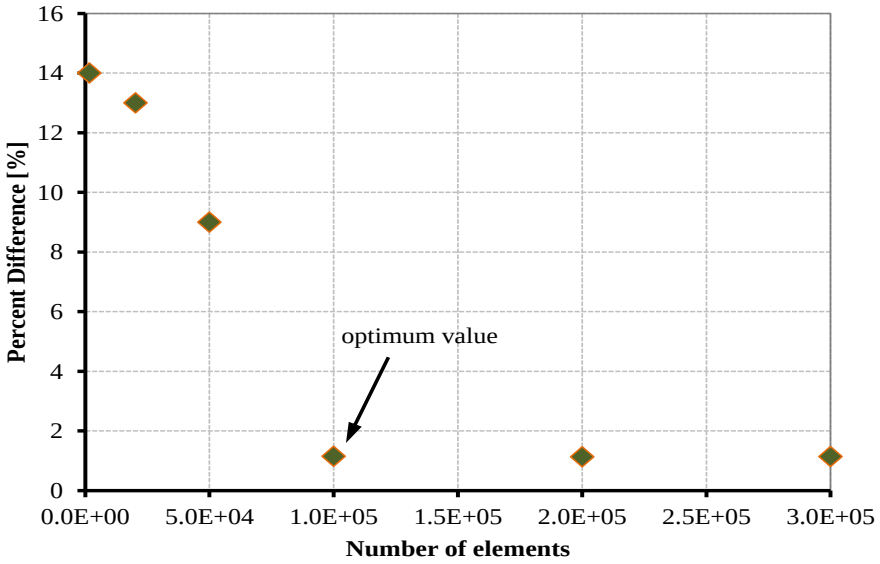

Figure 4.1: Mesh density analysis

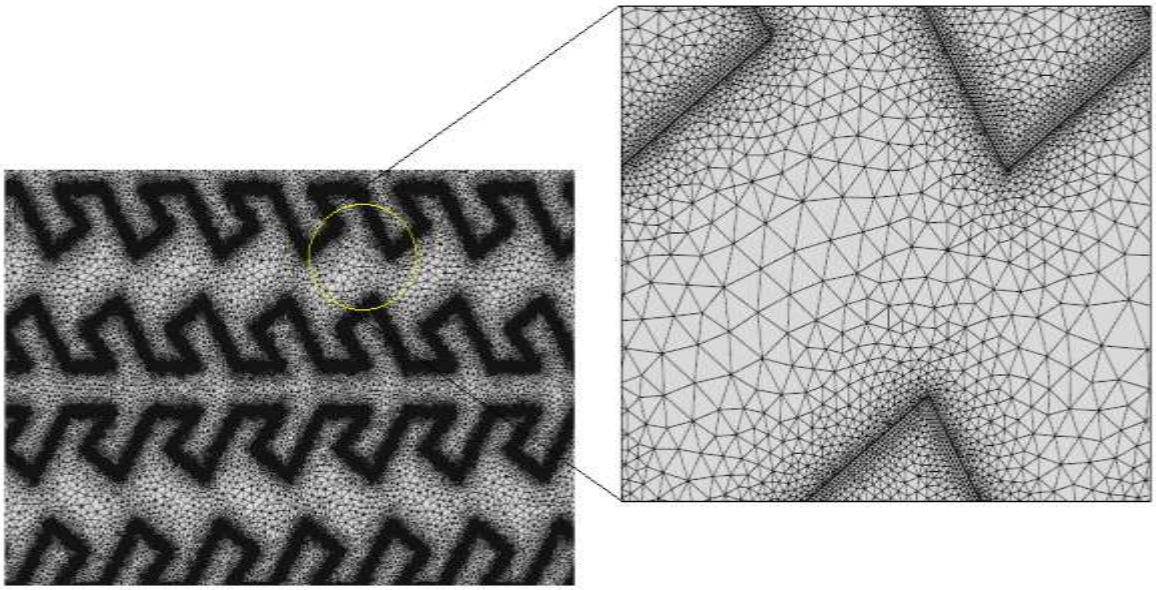

Figure 4.2: Example of meshing results for fish bone shaped comb driver

4.2 Spring Analysis

The simulation results are shown in Figure 4.3, against the theoretical calculations, which show good agreement. The simulation results indicate that the stiffness of the serpentine spring is 0.035 N/m, which correspond to a small 2.9% difference between the theoretical and simulation values for spring stiffness, which is acceptable. This difference believed to be due to the residual inaccuracy of the meshing.

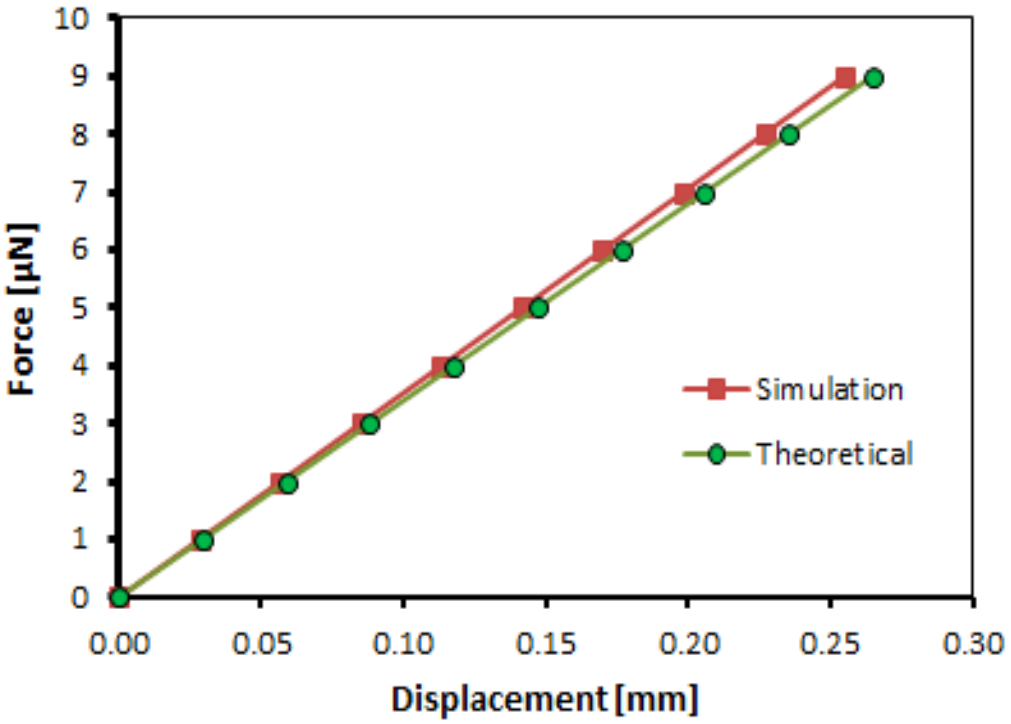

Figure 4.3: Simulation result of spring displacement with force applied

4.3 Simulation Validation for Conventional Electrostatic Comb Actuator

4.3.1 Summary case study by (Ye, Mukherjee, & MacDonald, 1998)

Figure 4.4 shows a schematic of conventional comb drive studied by Ye, Mukherjee, & MacDonald, 1998. For validation of our COMSOL simulation, the geometrical on dimension presented by Ye et al. were duplicated by us. The dimension are as follow: the minimum gap distance g is 1 μm, fixed electrode width W_f is 2 μm, and moving electrode width W_m is 1 μm. Fixed electrode is grounded whilst the moving electrode was applied with voltage potential range 0-100V.

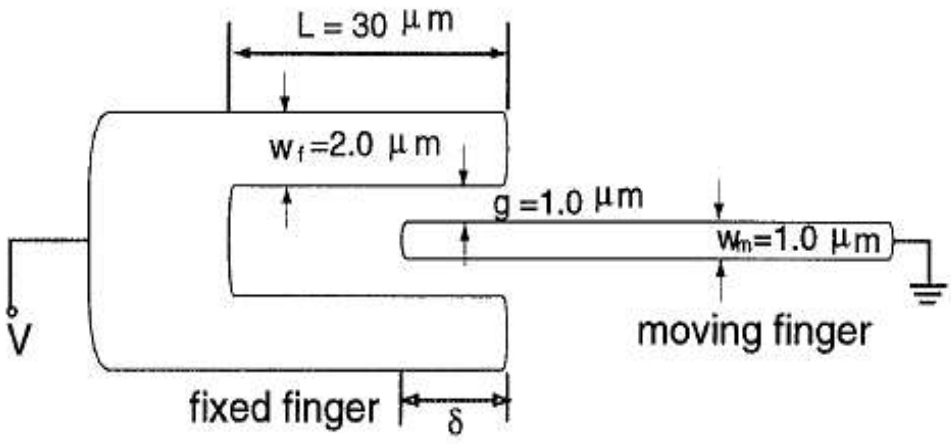

Figure 4.4: Schematic of single finger conventional comb drive

(Ye, Mukherjee, & MacDonald, 1998)

Ye et al. show numerical and aproximate approach for single finger actuator to calculate electrostatic force, described as follows: They proposed numerical result for the driving force, as a function of the distance traveled by the moving finger from the literature which are shown in Figure 4.5 where the relationship between electrostatic force F acting on the surface of the conductor is

$$F = \varepsilon \frac{hv^2}{g} \qquad \text{(Equation 24)}$$

This formula, was derived based on a capacitance model, where F is the driving force acting on a moving finger, h is the height of the fingers (in a direction normal to Figure 4.4), and v are the bias voltage and g is the gap between the fixed and moving fingers, respectively. Their results showed that the driving force remains constant if the gap and the height remain constant. According to the formula (Equation 24), the driving force can be a function of the distance traveled by a moving finger if the gap varies with distance. This provides the possibility of designing a variable-gap comb drive. The numerical example as shown in (Ye, Mukherjee, & MacDonald, 1998) also supports this possibility.

4.3.2 Validation of the simulations result with numerical results by (Ye, Mukherjee, & MacDonald, 1998)

In this section, explanation of our simulation as a validation comparison against the work done by Ye et al.(discussed in the previous section) will be provided. Refering to Figure 4.5, a plot of our results versus Ye et al. numerical results are compared. The difference between the two solutions is only 1.1%, which indicates good validation for the simulation result compared with the result from the literature. The slight deviation in the range of 5-20μm between this simulation and literature is due to the fact that the literature calculation was based on analytical methods i.e it did not take into consideration the lateral force and fringing force. Our force simulation consider this lateral force or fringing force, and hence is expected to be more accurate.

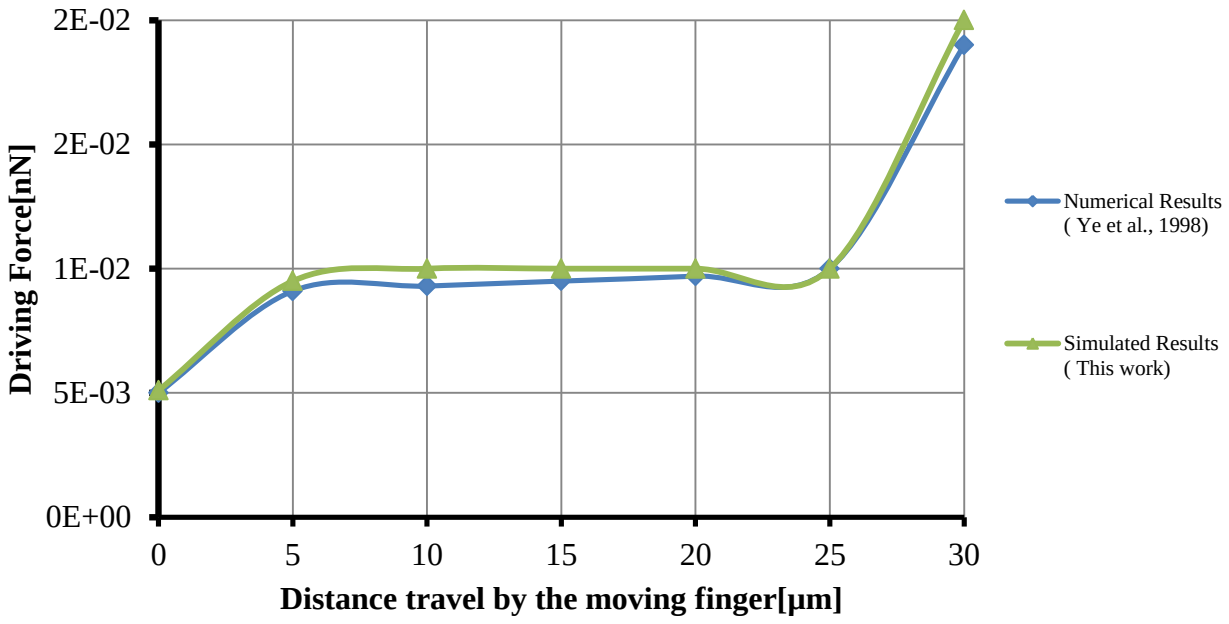

Figure 4.5: Electrostatic force as function of displacement

4.4 Comparison of Driving Force and Displacement for A Single Straight Sided and Fish Bone Electrostatic Comb Actuator

First, the performance of a single straight sided and fishbone actuator are compared in terms of its driving force and displacement upon application of an external voltage. For this simulation, an external voltage ranging from 0 V to 100 V was applied. Figure 4.6 shows the quadratic relationship between the electrostatic force acting vertically on a single straight sided comb finger and fishbone shaped comb driver, respectively, when external voltage is applied. For example, at 100 V driving external voltage, the drive force for fish bone shaped comb driver is 1364 % higher than the straight sided comb driver for a single finger.

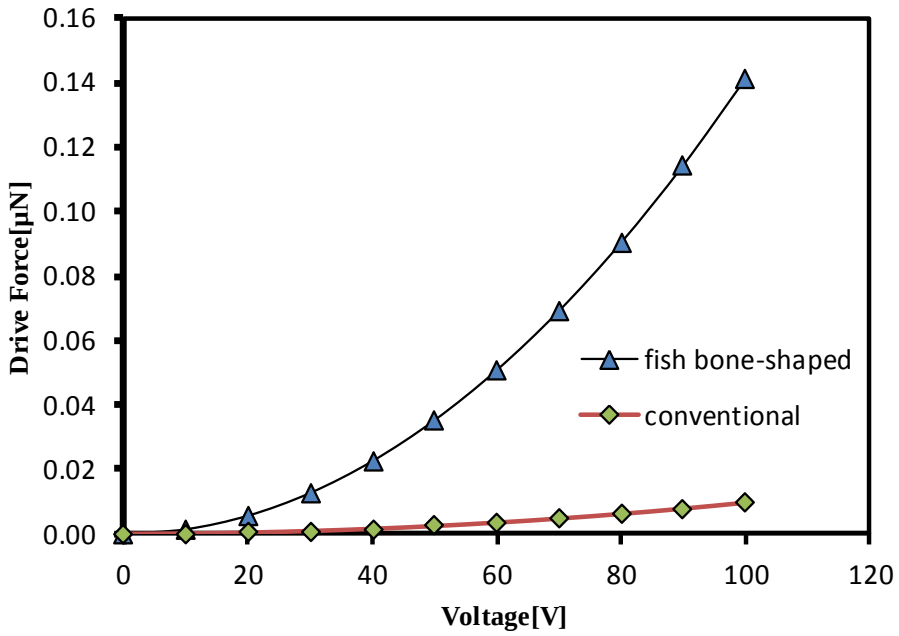

Figure 4.6: Electrostatic force (drive force) as a function of voltage, exerted on the comb fingers in the X direction for both single unit of straight sided comb finger and fish bone shaped comb driver

Figure 4.7 shows a comparison for the relationship between the electrostatic force and displacement, for a single straight sided comb finger and fishbone shaped comb finger. For 100 V, the improvement in displacement using the fishbone comb finger was 1364 %.

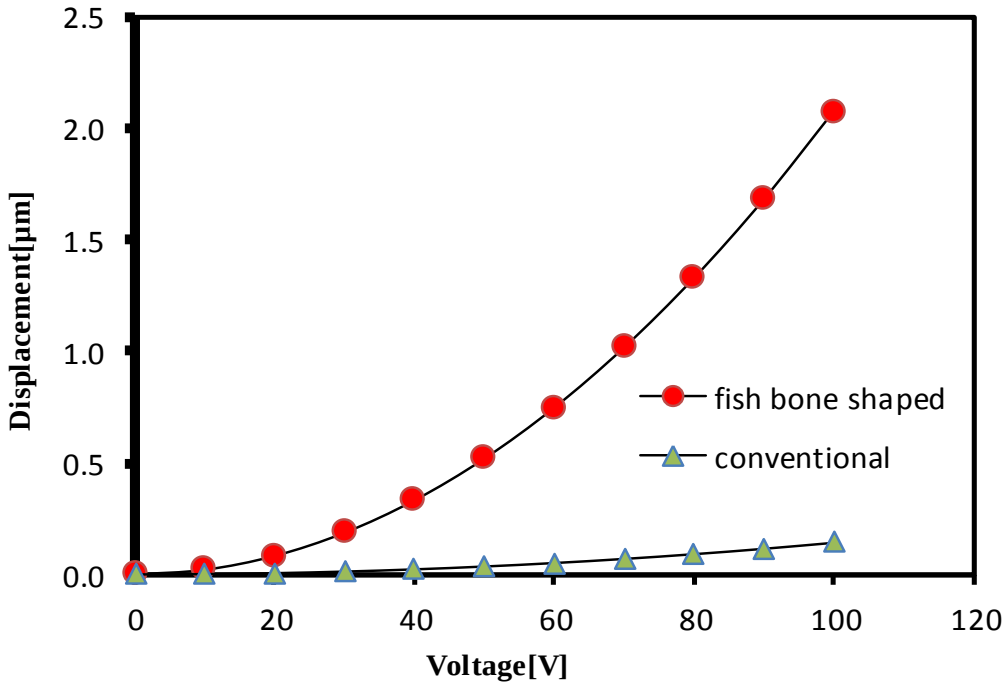

Figure 4.7: Driving voltage versus displacement of the comb fingers in the X direction for single unit of straight conventional comb finger and fishbone shaped comb driver

The improvement in displacement can be directly attributed to an understanding of the electric field distribution of the comb actuator geometry. The electric field distribution of the straight sided and fishbone actuators are shown in Figure 4.8 and Figure 4.9 respectively, in order to highlight the differences in the electrostatic field for both designs.

In the case of the straight sided actuator shown in Figure 4.8, it can be seen that the electric field is concentrated at the corners of the straight comb finger. The magnitudes of the electrostatic forces on the static and dynamic electrodes are in equal but opposite in directions, thus, a cancelling out of the forces in the y direction. The only remaining forces are at the corners of the fingers, which the largest forces or more are commonly known as fringing forces that ultimately serve as the main driving force of the straight sided electrostatic comb driver.

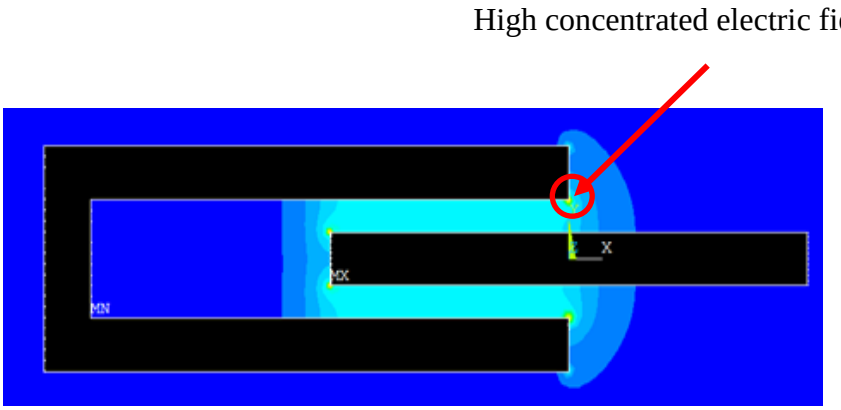

Figure 4.8: Electric field distribution of single finger straight electrostatic conventional comb drive actuator

In comparison, the fish bone shaped comb drive actuator shown in Figure 5.7, produces many more strong electrostatic fringing forces, due to the many sharp edges of the actuator geometry. These highly concentrated electric field regions can be referred to in Figure 5.7.

Furthermore, since these small fingers are placed at an angle to the backbone, the resultant electrostatic fields have components in both the X and Y directions. Whilst the forces in the Y directions will cancel out similar to the case of the straight sided comb actuator, the components in the X directions and added up to form strong driving force in the X direction. This increase in forces due to the fishbone geometry is responsible for the significant increase in actuation force and displacement for the fishbone geometry.

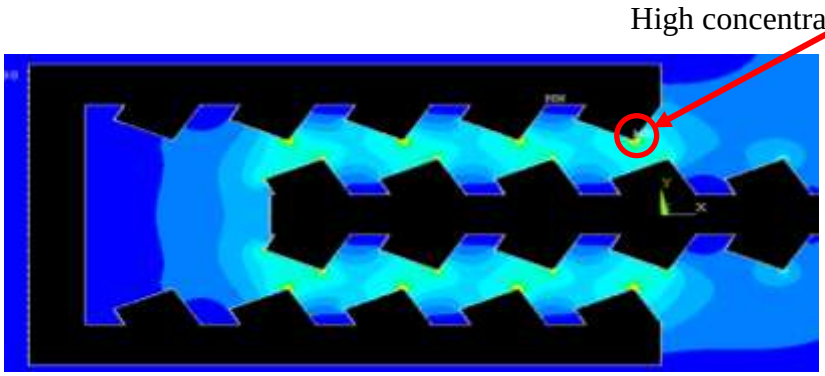

Figure 4.9: Electric field distribution of single finger fish bone shaped electrostatic comb drive actuator

4.5 Comparison of Driving Force and Displacement for Multiple Fingers Straight Sided and Fishbone Electrostatic Comb Actuator

The performance of an array of straight sided and fishbone actuator, contained with an equivalent active area (of 800 x 300 μm^2) are compared in terms of its driving force and displacement upon application of an external voltage. For this simulation, an external voltage ranging from 0 - 100 Volts was applied. Figure 5.10 shows the relationship between the electrostatic force acting vertically on a single straight sided comb finger and fishbone shaped comb driver, respectively, when external voltage is applied. For example, at 100 V driving external voltage, the drive force for fish bone shaped comb driver is 485 % higher than the straight sided comb driver for a single finger.

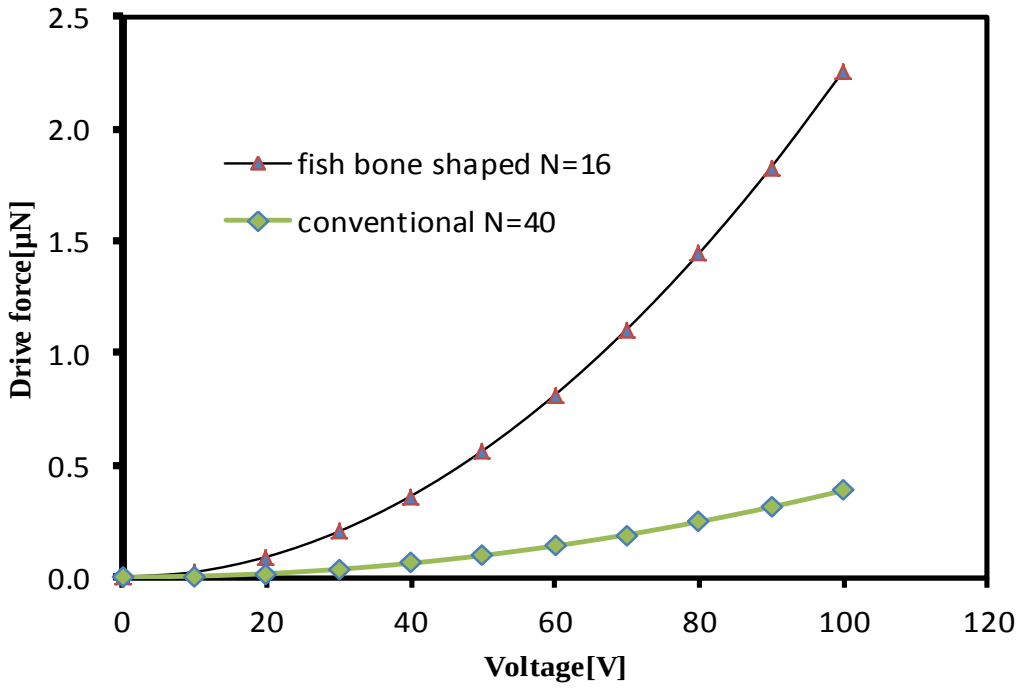

Figure 4.10: The relationship between driving voltage and electrostatic force exerted on the comb fingers in X direction for both multiple fingers of straight conventional comb driver and fish bone shaped comb driver

Similarly, Figure 4.11 shows a comparison for the relationship between the electrostatic force and displacement, for a single straight sided comb finger and fishbone shaped comb finger. For 100 V, the improvement in displacement using the fishbone comb finger was 485 %, due to the use of the same spring constant.

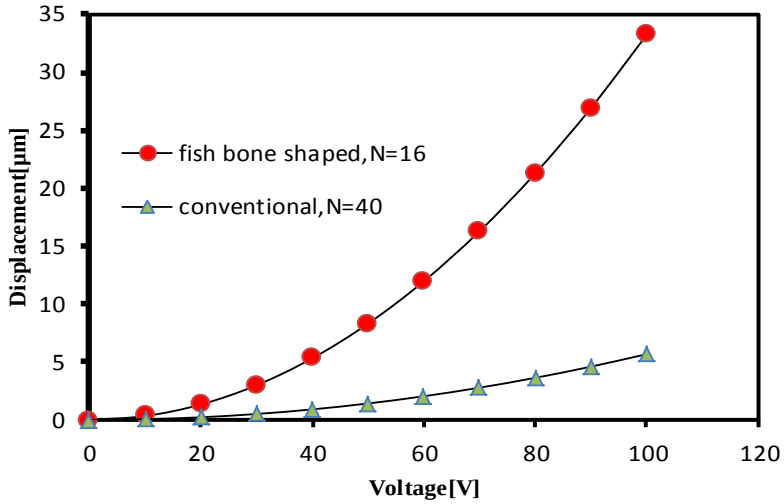

Figure 4.11: The relationships between a driving voltage and displacement of the comb fingers in X direction for both multiple fingers of straight conventional comb driver and fish bone shaped comb driver

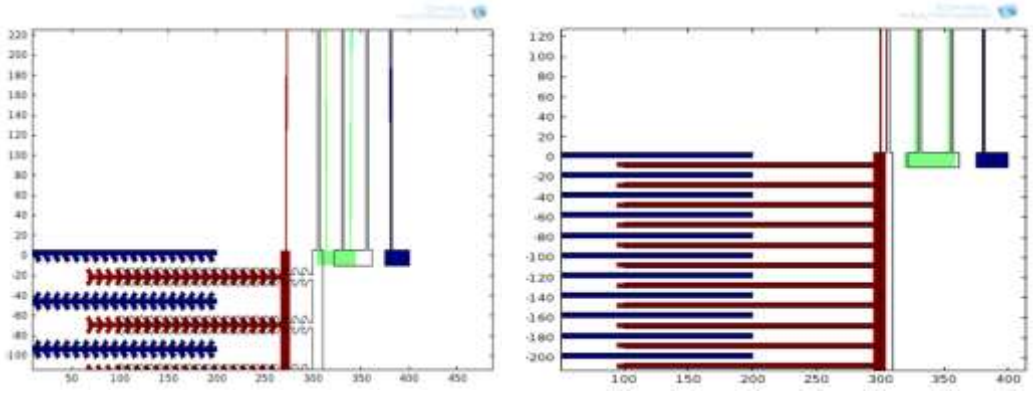

a) b)

Figure 4.12: Deformation distribution of actuators (a) fishbone shaped and (b) conventional

Figure 4.13 shows the simulation result of the electrostatic force acting versus finger engagement for both single finger of conventional straight sided comb driver and single finger of the fishbone shaped comb driver with voltage applied at 100 volts. As expected, the trend of the conventional of straight sided comb driver shows constant force output over the range of engagement as validated by (Jensen, Mutlu, Miller, Kurabayashi & Allen, 2003) in the earlier work. However, for a single finger of the fishbone shaped comb driver, the graph shows that the electrostatic forces produce experienced a stepped a rate of change with respect to the finger engagement based on the points of inflection produced by the design. However, the design still demonstrated a negative force effect after every step of maximum force, where the negative gradients of forces occur in certain finger engagement which results from the spacing between the small fingers within the electrodes.

It is significant to note that the characteristic behavior of the electrostatic force of this fishbone actuator, as a function of displacement results in a periodic variation with regards to distance. This is identified as a "cogging effect", as shown in Figure 4.13. This cogging effect may be linearized, or manipulated to other force-displacement profiles (such as a stepped profile) through manipulation of the electrode arrays.

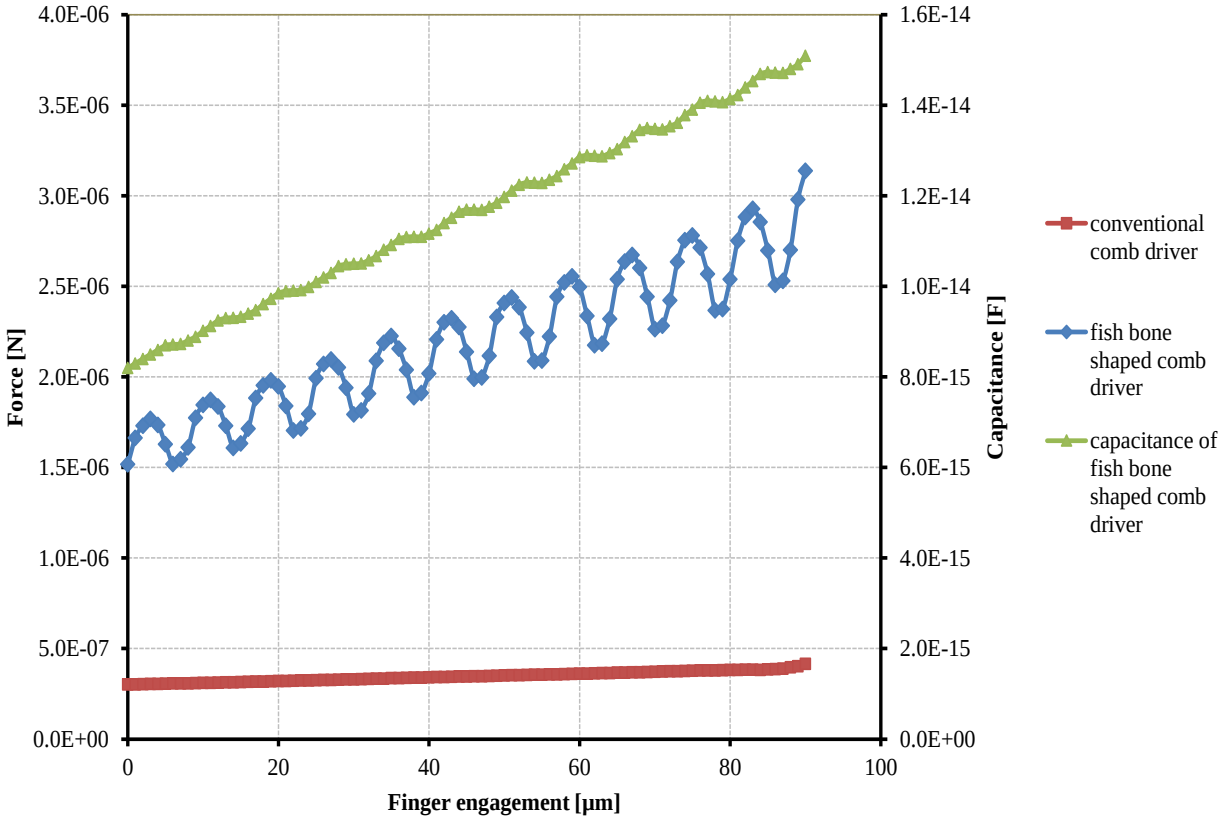

Figure 4.13: Force versus finger engagements and capacitance versus finger engagement

4.6 Fishbone Shaped Comb Drive Design Variations Effects on Force Generated by Fish Bone Shaped Comb Driver

The force profile of the fish bone shaped comb driver does not change by varying *r*. As shown in Figure 4.14, the maximum force generated is inversely proportional to *r*. The amount of finger engagement required to complete one cycle is proportional to r.

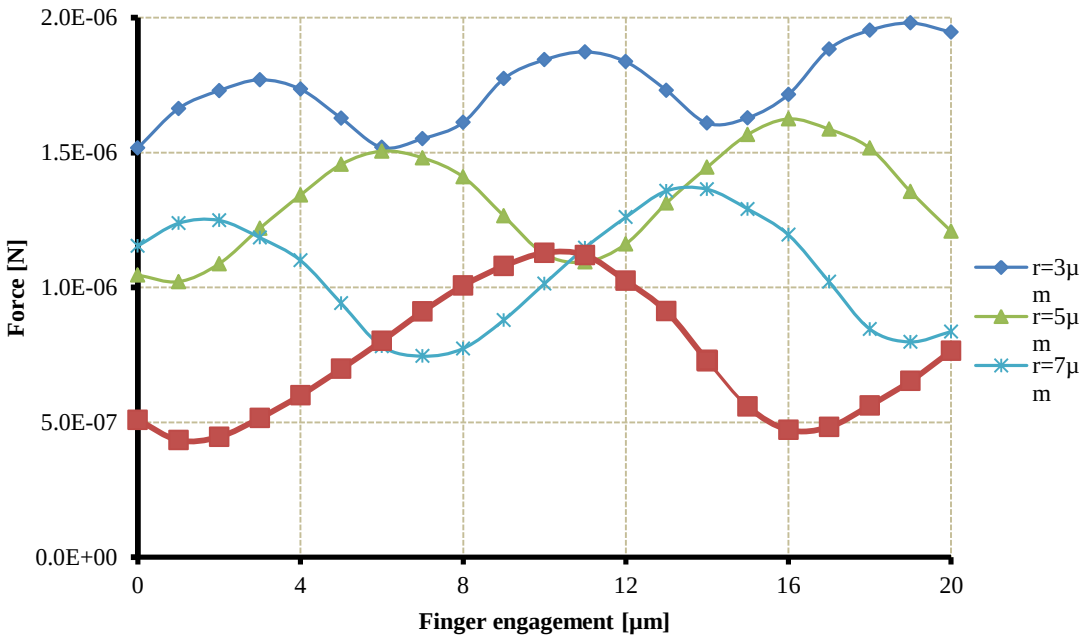

Figure 4.14: The effect of r small finger separation, on force versus finger engagement

For this study, the effect of the angle to the force generated by the comb drive over finger engagement was simulated , for a range of angles ɵ°= 0°, 5°, 13°, 20°, 46°. Result in Figure 4.15 show that the electrostatic force increases with an increase in angle ɵ°, but seems to approach a plateau as it reaches 46°.

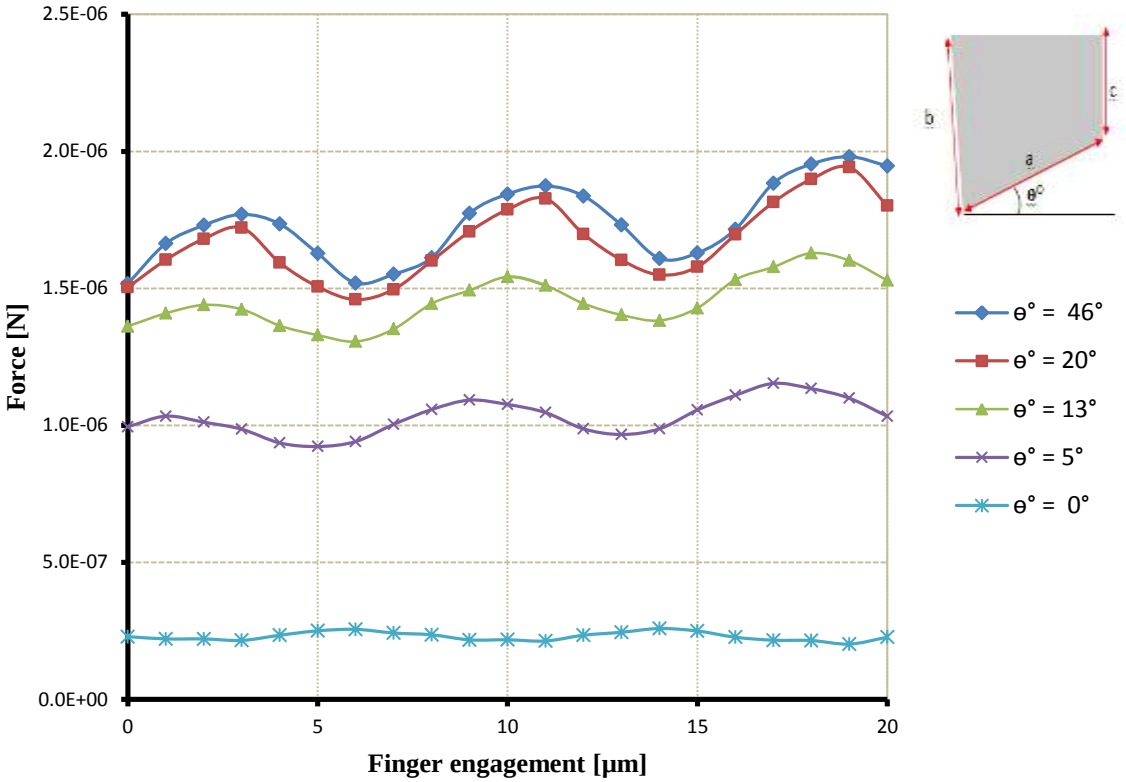

Figure 4.15: Force versus finger engagements effects on variation of angle, ɵ°

The original design (a, b, c = 5, 5, 3) shows the highest force generated as shown in Figure 4.16, the inverse of the original design (a, b, c = 3, 3, 5) produces force in the opposite direction. Similarly, for (a, b, c = 3, 4, 4) and its inverse design shows an identical trend, although the force generated is slightly lower. When the angle is 0° (a, b, c= 4, 4, 4), low constant force is generated similar to the force output of a conventional comb driver.

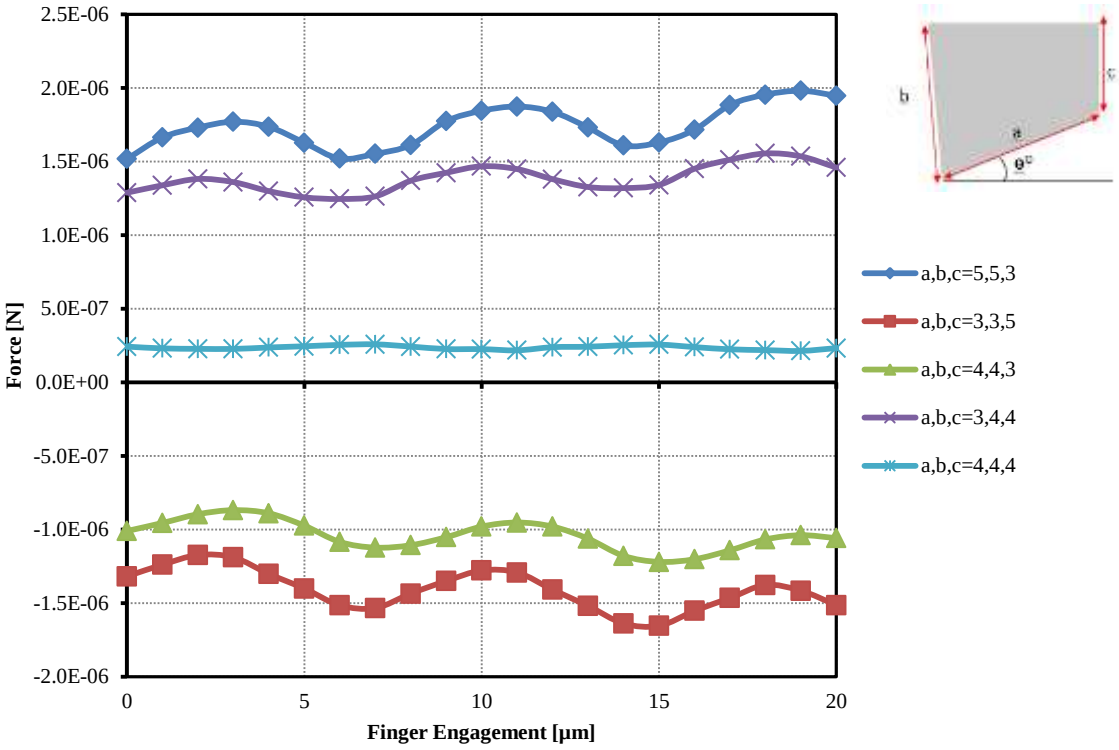

Figure 4.16: Force versus finger engagements effect on variations of parameter a, b, and c

4.7 Design to Overcome Negative Force "Cogging Effects"

The graph in Figure 4.17 shows force versus finger engagement ranging from 0-20μm of the fishbone shaped comb. Figure 4.17 shows that the trend of the force versus finger engagement did not change at all by increasing the number of comb fingers, whereas the negative gradient of force with respect to the finger engagement was still occurring for every maximum point of the step force.

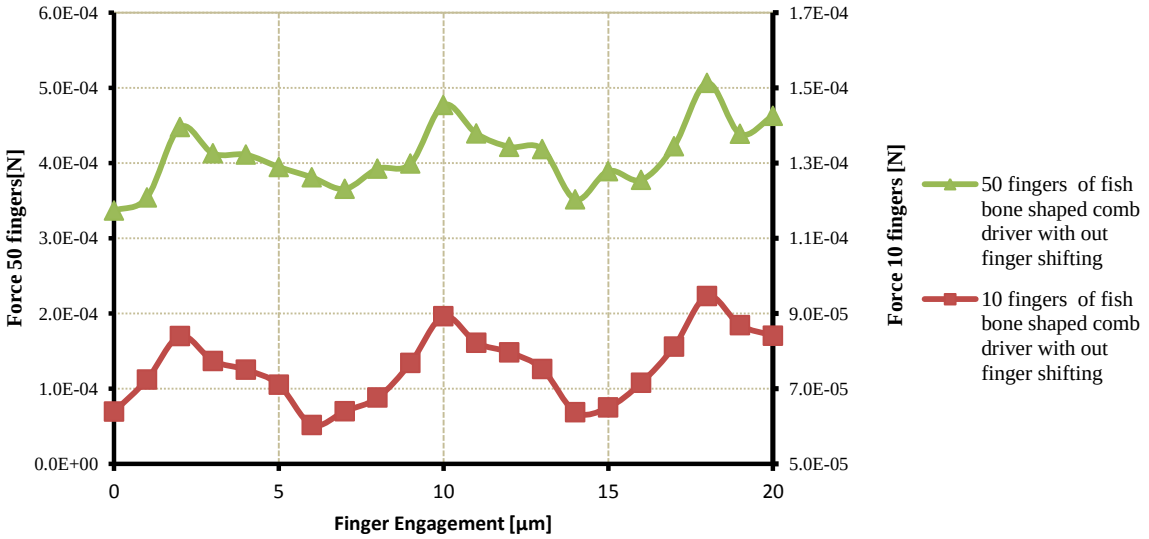

Figure 4.17: Force versus finger engagement effects upon variation of the number of comb fingers, n

Figure 4.18 shows that after application of the finger shifting method to the fishbone comb array, a smoothing of the translational motion is achieved for$F_s = (^8/_7)(n)$. The key advantage of the finger shifting method is as follows: without the finger shifting method, a large number of fingers would result in a larger driving force. However, the minimum positions which indicate the cogging effect would persist.

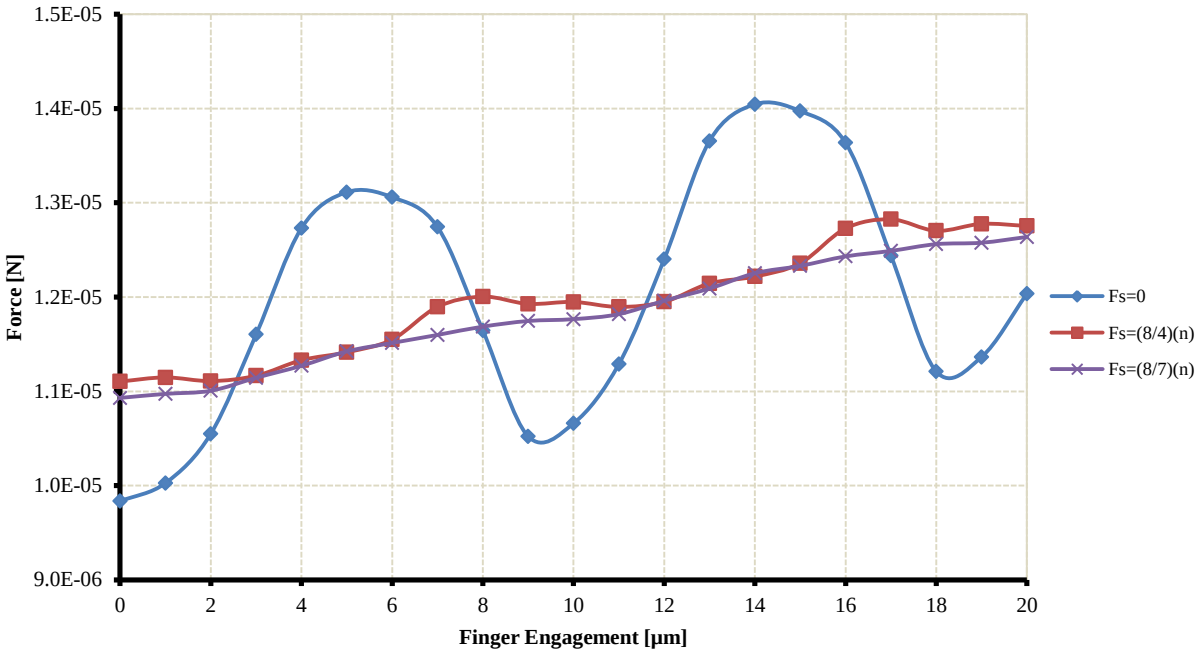

Figure 4.18: Force versus finger engagement profile upon variation of the finger shifting value $F_s(n)$

With the finger shifting method, these minimum positions would cancel out, and the resultant force would be smoothened out. In this case, resultant electrostatic forces now linearly increase in the same direction as shown in Figure 4.19.

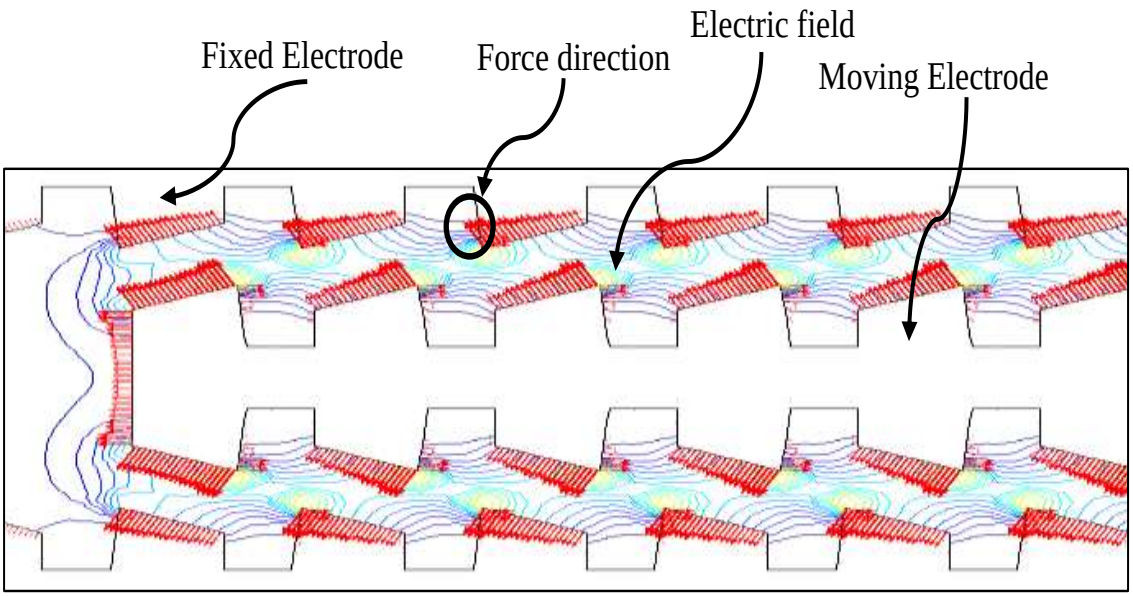

Figure 4.19: Electrostatic force direction of fishbone shaped comb driver

CHAPTER 5

CONCLUSION

This study introduces a high force density fishbone shaped electrostatic comb drive actuator. Hence, it is able to exert a high force in a relatively small active area, thus rendering it attractive in miniaturized applications such as micro tweezers and micro grippers. This work had discussed the design of a fishbone shaped electrostatic actuator, and compared its performance with a straight sided electrostatic actuator. Comparison in terms of driving force and displacement as a function of voltage was presented giving an improvement 1364 % for a single actuator operating at 100 V, and 485 % improvement on the performance for a similar active area of electrostatic actuator. This indicates that this fishbone design has potential as a high density electrostatic actuator, which is a solution to the large active area which challenges most designs related to electrostatic actuator. This high force density is enabled through the branched structure of fishbone actuator geometry, which increases the driving force along the longitudinal axis of the actuator, and at the same time minimizes any crosstalk in the transverse y direction. However, the electrostatic force profiles as a function of the translational distance show a cogging effect. This cogging effect is caused by the negative force profile, and acts opposite to the translational motion, thus reducing the overall force and causing a periodically varying force-displacement profile in the desired translational direction. As a solution, the finger shifting method was introduced. Through superposition, the local minima caused by the negative force profile are canceled out through graduated placement of the interdigitated fishbone fingers. The resulting electrostatic force is positive and close to linear, ensuring smooth actuation. For desired actuation application, the finger shifting method may be adapted to produce step-like or ramp-like electrostatic actuation profile.

Based on the results analysis in chapter 4, Table 5 shown the parameters of the basic fishbone shaped comb drive concluded in this study as the best parameter from the variations parameters tested and simulated in this study to perform high force density electrostatic comb drive actuator which having high potential for micro tweezers or micro gripper applications. For future work, fabrication for the fish bone shaped actuator design based on the parameter concluded in table 5 is recommended for validation.

Table 5 Parameters of basic fishbone shaped comb drive

Parameters	Value
Minimum gap, *g*	3 µm
Overlap length, O_L	100 µm
Width, *w*	5 µm
Small finger separation, *r*	3 µm
Finger length, *L*	215 µm
Number of small finger, *N*	25
Angle, **ɵ°**	46°
Length of *a*, *b*, *c* and *d*	5 µm, 5 µm, 3 µm

APPENDIX A

PUBLICATIONS

Megat Hasnan, M. M. I., Mohd Sabri, M. F., Said, S.M., & Nik Ghazali, N. N., (2014). Modeling of a High Force Density Fishbone Shaped Electrostatic Comb Drive Microactuator. The Scientific World Journal, 2014.

CONFERNCES

Megat Muhammad Ikhsan Bin Megat Hasnan, Mohd Faizul Bin Sabri, Suhana Mohd Said: "Design And Simulation Of High Force Density Electrostatic Comb Drive Actuator ", oral presentation at the 6th International Conference on Sensors (ASIA SENSE 2013) Melaka, Malaysia, p45, 2013.

PATENT

PT/4272/UM/12, FISHBONE ELECTROSTATIC COMB DRIVE ACTUATOR, UNIVERSITY MALAYA

REFERENCE

Ahmed H, Moussa WA. (2003). Optimizing The Performance of Electrostatic Comb-Drive Actuators Using Neural Networks. *In Proc. Intl. Conf. on MEMS, NANO and Smart Syst* 62-68.

Abarca-Jiménez, G. S., Reyes-Barranca, M. A., Mendoza-Acevedo, S., Munguía-Cervantes, J. E., & Alemán-Arce, M. A. (2015). Electromechanical modeling and simulation by the Euler–Lagrange method of a MEMS inertial sensor using a FGMOS as a transducer. *Microsystem Technologies*, 1-9.

Bell, D., Lu, T., Fleck, N., Spearing, S. (2005). MEMS Actuators and Sensors: Observations on Their Performance and Selection for Purpose. *J of Micromech Microeng*, S153.

Bronson, J.R. (2007). Modeling and Control of MEMS Micromirror Arrays With Nonlinearities and Parametric Uncertainties, *Dissertation Doctor of Philosophy University of Florida.*

Beyeler, F., Bell, D. J., Nelson, B. J., Sun, Y., Neild, A., Oberti, S., & Dual, J. (2006, October). Design of a Micro-gripper and an Ultrasonic Manipulator for Handling Micron Sized Objects. *IEEE/RSJ International Conference in Intelligent Robots and Systems*, 772-777.

Chiou, J.C., Kuo, C.F., Lin, Y.J., Chang, CW, Hou KC. (2008*).* Development Of Novel Cascade Structure For Improving Stroke Of Electrostatic Comb-drive Actuator. *In IEEE 21st Intl Conf on Microelectromech Syst*.

Chow J, Lai Y. (2009). Displacement Sensing of a Micro-electro-thermal Actuator Using a Monolithically Integrated Thermal Sensor. *Sensors and Actuators A*, 150 137.

Conway, N.J., Kim, S.G. (2004). Large-strain Piezoelectric In-plane Micro-actuator. *In Proc IEEE Micro Electro Mech. Syst*, 454-457.

Chyuan, S.W., Liao, Y.S., Chen, J.T.(2005). Computational Study of The Effect of Finger Width and Aspect Ratios for The Electrostatic Levitating Force Of MEMS Comb Drive, *IEEE J. Microelectromech. Syst. 14, 2*, 305–312.

Comsol, A. B. (2005*). COMSOL multiphysics user's guide*. Version: September.

Defeng, L. (2008). A Study on Micro-gripping Technologies, *Doctorate thesis, Delft.*

Dafflon, M., Lorent, B., Clavel, R., Beyeler, F. & Nelson, B. (2006). Characterization of Micro Manipulation Tasks Operated with Various Controlled Conditions by Micro Tweezers, *Proc. of International Workshop on Microfactories*.

Eleftheriou, E., Antonakopoulos, T., Binnig, G., Cherubini, G., Despont, M., Dholakia, A., Durig, U., Lantz, M., Pozidis, H., & Rothuizen, H. (2003). Millipede-a MEMS-Based Scanning-probe Data-storage System Magnetics, *IEEE Transactions 39*, 938-945.

Engelen, J., Lantz, M., Rothuizen. H., Abelmann, L., Elwenspoek, M. (2009). Improved Performance of Large Stroke Comb-drive Actuators by using a Stepped Finger Shape. *In Proc. of the Transducers*, 1762-1765.

Grade, J..D., Jerman, H., Kenn, T.W. (2003). Design of Large Deflection Electrostatic Actuators. *J Microelectromech Syst 12*, 335-343.

Horsley, D.A., Wongkomet, N. R., Horowitz & Pisano. (1999). A.P. Precision Positioning using a Microfabricated Electrostatic Actuator, *IEEE Transactions on Magnetics ,35.* 993-999.

Hu, W., Hu, G., Wei, X., Xie, X. (2010). Modeling and Simulation of Electrostatic Comb-drive Actuators with Modelica. *In Proc. In Intl. Conf. on Measuring Technology and Mechatronics Automation (ICMTMA)*, 679-682.

Harouche, I.P., Shafai, C. (2005). Simulation of Shaped Comb Drive as a Stepped Actuator for Microtweezers Application. *Sensors and Actuators A 123*, 540-546.

Jaecklin, V.C., Linder, De Rooij, N., & Moret, J. (1992). Micromechanical Comb Actuators with Low Driving Voltage, *Journal of Micromechanics and Microengineering, 2*, 250.

Jensen, B.D., Mutlu, S., Miller, S., Kurabayashi, K., & Allen, J.J. (2003). Shaped Comb Fingers for Tailored Electromechanical Restoring Force, *Journal of Microelectromechanical Systems ,12*, 373-383.

Kalicinski, S., Tilmans, H. A. C., Wevers, M., & De Wolf, I. (2009). A New Characterization Method for Electrostatically Actuated Resonant MEMS: Determination of The Mechanical Resonance Frequency, Quality Factor and Dielectric Charging. *Sensors and Actuators A: Physical, 154(2)*, 304-315.

Kim, C.J, Pisano, A.P, Muller, R.S., & Lim, M.G.(1992). Polysilicon Microgripper, *Sensors and Actuators A-Physical ,33*, 221-227.

Krishnan, S., Saggere, L. (2012). Design and Development of a Novel Micro-class Gripper for Micromanipulation of Complex-shaped Objects. *Sensors and Actuators A 176*, 110-123.

Lantz, M.A., Rothuizen, H.E., Drechsler, U., Haberle, W., Despont, M. (2007). A Vibration Resistant Nanopositioner for Mobile Parallel-probe Storage Applications. *J Microelectromech Syst 16*, 130-139.

Liu, C.H., Kenny, T.W. (2001). A high-precision, Wide-bandwidth Micromachined Tunneling Accelerometer. *J Microelectromech. Syst 10*, 425-433.

Lagouge, M., & Discovering, M. E. M. S. (2009). *Microtechnology*.

Legtenberg, R., Groeneveld, A., Elwenspoek, M. (1996). Comb-drive Actuators for Large Displacements. *J Micromech Microeng 6*, 320.

Multiphysics, C. O. M. S. O. L. (2012). 4.3 *User's Guide*.

Olfatnia, M., Sood, S., Gorman, J.J., Awtar, S. (2013). Large Stroke Electrostatic Comb-Drive Actuators Enabled by a Novel Flexure Mechanism. *J Microelectromech Syst 22*, 483-494.

Osonwanne, N., Clark, J.V. (2010). MEMS Comb Drive Gap Reduction Beyond Minimum Feature Size: A Computational Study. *In Proc. Conf. COMSOL 2010*.

Rivlin, B., & Elata, D. (2012). Design of Nonlinear Springs for Attaining a Linear Response in Gap-closing Electrostatic Actuators, *International Journal of Solids and Structures, 49*, 3816-3822.

Rodgers, M.S., Kota, S., Hetrick, J., Li, Z., Jensen, B. D., Krygowski, T.W., Miller, S.L., Barnes, S.M., & Burg, M.S. (2000). A New Class of High Force, Low-voltage, Compliant Actuation Systems, *Proc. Solid-State Sensor and Actuator Workshop,* 210-213.

Rosa, M.A., Dimitrijev, S., & Harrison, H.B. (1998). Enhanced Electrostatic Force Generation Capability of Angled Comb Finger Design Used in Electrostatic Comb-drive Actuators, *Electronics Letters ,34*, 1787-1788

Sun, Y., Nelson, B.J., Potasek, D.P., & Enikov, E. (2002). A Bulk Microfabricated Multi-axis Capacitive Cellular Force Sensor using Transverse Comb Drives. *J Micromech Microeng 12*,832.

Sabri, M.F.M., Ono, T., Esashi, M. (2009). Modeling and Experimental Validation of the Performance of a Silicon XY-microstage Driven by PZT Actuators. *J of Micromech Microeng 19*, 095004.

Shakoor, R., Chughtai, I., Bazaz, S., Hyder, M. (2005). Numerical Simulations of MEMS Comb-Drive using Coupled Mechanical and Electrostatic Analyses, *In Proc. 17th Intl. Conf. Microelectronics.*

Sabri, M.F.M., Ono, T., S.M. Said, Y. Kawai, M. Esashi, Fabrication and Characterization of Microstacked PZT Actuator for MEMS Applications. (2014). *Journal of Microelectromechanical Systems. 99*.

Sabri, M.F.M, Ono, T., Esashi, M. (2009). Modeling and Experimental Validation of The Performance of a Silicon XY Microstage Driven by PZT actuators, *Journal of Micromech Microeng. 19*, 9.1651-1654.

Seeger, J.I., & Boser, B.E. (2003). Charge Control of Parallel-plate, Electrostatic Actuators and The Tip-instability, *Journal of Microelectromechanical Systems. 12*, 656-671.

Sharma, J., & DasGupta, A. (2009). Effect of Stress on The Pull-in Voltage of Membranes for MEMS Application. *Journal of Micromechanics and Microengineering, 19, 11*, 115021.

Tsay, J., Su, L.Q., Sung, C.K. (2005). Design of a Linear Micro-feeding System Featuring Bistable Mechanisms. *J Microelectromech Syst 15*, 63.

Tang, W.C., Lim, M.G., Howe, R.T. (1992). Electrostatic Comb Drive Levitation and Control Method, *IEEE J. Microelectromech. Syst. 1, 4*, 170–178.

Tang, W.C., Nguyen, T.C.H., & Howe, R.T. (1989). Laterally Driven Polysilicon Resonant Microstructures, *Sensors and Actuators 20*, 25-32.

Tang, W.C., Nguyen, T.C.H., Judy, M.W., Howe, R.T. (1990). Electrostatic-comb drive of lateral polysilicon resonators, *Sensor. Actuat. A21–23*, 328–331.

Tsay, J., Su, L. Q., & Sung, C. K. (2005). Design of a Linear Micro-feeding System Featuring Bistable Mechanisms. *Journal of Micromechanics and Microengineering, 15(1)*, 63.

Wang, J., Yang, Z., Yan, G. (2012*).* Silicon-on-Insulator Out-of-plane Electrostatic Actuator with in situ Capacitive Position Sensing, *J Micro/Nanolithography MEMS and MOEMS 11,* 033006.

Wang, Z., Shen, X., & Chen, X. (2015). Design, modeling, and characterization of a MEMS electrothermal microgripper. *Microsystem Technologies*, 1-8.

Wierzbicki, R., Houston, K., Heerlein, H., Barth, W., Debski, T., Eisinberg, A., Menciassi, A., Carrozza, M. C., & Dario, P. (2006). Design and fabrication of an electrostatically driven microgripper for blood vessel manipulation, *Microelectronic Engineering, 83,*

Volland, B.E., Heerlein, H., & Rangelow, I. W. (2002). Electrostatically Driven Microgripper, *Microelectronic Engineering, 61-2,* 1015-1023

Varadan, V. K., Vinoy, K. J., & Jose, K. A. (2003). RF MEMS and Their Applications. John Wiley & Sons.

Ye, W.J., Mukherjee, S., & MacDonald, N.C. (1998). Optimal Shape Design of an Electrostatic Comb Drive in Microelectromechanical Systems, *Journal of Microelectromechanical Systems , 7,* 16-2.